SC5295.3AR

STRENGTHENING AND STRENGTH UNIFORMITY OF STRUCTURAL CERAMICS

ANNUAL REPORT FOR THE PERIOD
February 1, 1983 through January 31, 1984

CONTRACT NO. F49620-81-C-0036

Prepared for

Air Force Office of Scientific Research
Directorate of Electronic and Material Sciences
Building 410
Bolling Air Force Base, DC 20332

F.F. Lange
Principal Investigator

APRIL 1984

Rockwell International
Science Center

UNCLASSIFIED
SECURITY CLASSIFICATION OF THIS PAGE

AD-A144302

REPORT DOCUMENTATION PAGE

1a. REPORT SECURITY CLASSIFICATION Unclassified	1b. RESTRICTIVE MARKINGS
2a. SECURITY CLASSIFICATION AUTHORITY	3. DISTRIBUTION/AVAILABILITY OF REPORT Approved for public release; distribution unlimited.
2b. DECLASSIFICATION/DOWNGRADING SCHEDULE	
4. PERFORMING ORGANIZATION REPORT NUMBER(S) SC5295.3AR	5. MONITORING ORGANIZATION REPORT NUMBER(S) AFOSR-TR- 84-0606
6a. NAME OF PERFORMING ORGANIZATION Rockwell International Science Center 6b. OFFICE SYMBOL (If applicable)	7a. NAME OF MONITORING ORGANIZATION AFOSR/NE
6c. ADDRESS (City, State and ZIP Code) 1049 Camino Dos Rios Thousand Oaks, California 91360	7b. ADDRESS (City, State and ZIP Code) Bldg 410 Bolling AFB DC 20332
8a. NAME OF FUNDING/SPONSORING ORGANIZATION Air Force Office of Scientific Research 8b. OFFICE SYMBOL (If applicable) NE	9. PROCUREMENT INSTRUMENT IDENTIFICATION NUMBER Contract No. F49620-81-C-0036
8c. ADDRESS (City, State and ZIP Code) Building 410 Bolling Air Force Base, DC 20332	10. SOURCE OF FUNDING NOS. PROGRAM ELEMENT NO.: 61102F PROJECT NO.: 2306 TASK NO.: A2 WORK UNIT NO.:
11. TITLE (Include Security Classification) STRENGTHENING AND STRENGTH UNIFORMITY OF STRUCTURAL CERAMICS (U)	
12. PERSONAL AUTHOR(S) Lange, Fred F.	
13a. TYPE OF REPORT Annual Report 13b. TIME COVERED FROM 02/01/83 TO 01/31/84	14. DATE OF REPORT (Yr., Mo., Day) APRIL 1984 15. PAGE COUNT 75
16. SUPPLEMENTARY NOTATION	
17. COSATI CODES FIELD / GROUP / SUB. GR.	18. SUBJECT TERMS (Continue on reverse if necessary and identify by block number)

19. ABSTRACT (Continue on reverse if necessary and identify by block number)

APPENDIX IV: Organic inclusions (e.g., lint) produce irregular-shaped voids observed at fracture origins. These voids can be eliminated from a powder compact by a presintering processing step: organic burn-out at a temperature prior to bulk shrinkage and iso-pressing at room temperature. This procedure was demonstrated for the case of voids produced by polystyrene spheres (4 to 100 μm diameter).

APPENDIX V: A preliminary study was undertaken to determine if EDAX spectra, obtained at different magnifications, might be used to define the phase distribution in a multiphase material. Al_2O_3/ZrO_2 composites were used for the study. EDAX spectra were acquired for a number of arbitrarily selected areas at each magnification using a commercial scanning electron microscope/x-ray detector/multichannel analyzer system. A statistical analysis of the spectra showed that the deviation from the mean phase distribution increased with magnification. These results showed that the smallest area that contained the same phase distribution as the whole specimen could be defined if one first defines an acceptable deviation from the mean. Spectra acquired for the same area suggest that an acceptable deviation is 5% of the mean. Within the limits of multi-

20. DISTRIBUTION/AVAILABILITY OF ABSTRACT UNCLASSIFIED/UNLIMITED ☒ SAME AS RPT. ☐ DTIC USERS ☐	21. ABSTRACT SECURITY CLASSIFICATION Unclassified
22a. NAME OF RESPONSIBLE INDIVIDUAL Mr Coplan (IVAN)	22b. TELEPHONE NUMBER (Include Area Code) 202-767-4933 22c. OFFICE SYMBOL NE

DD FORM 1473, 83 APR EDITION OF 1 JAN 73 IS OBSOLETE.

UNCLASSIFIED
SECURITY CLASSIFICATION OF THIS PAGE

SC5295.3AR

PROGRAM SUMMARY

The goal of this work is to identify the processing flaws that limit the strength of sintered ceramics, and to engineer uniform microstructures which either eliminate or minimize the size of these processing flaws. During the first year, a major advance was made by uncovering the fact that agglomerates in powders produce crack-like voids that severely limit the strength of sintered ceramics. Crack-like voids produced by the differential sintering of agglomerates relative to their surrounding powder matrix can be the most detrimental strength degrading flaw in sintered ceramics. As detailed and summarized in the review prepared for a 1984 ASM Conference on Materials for Future Energy Systems, colloidal approaches to powder processing and consolidation can minimize the size of soft agglomerates (those that can be broken apart with surfactants) and hard agglomerates (eliminated by sedimentation of colloidal suspensions). Work has shown that the elimination of the large, soft agglomerates with surfactants increases the average strength of a transformation toughened Al_2O_3/30 v/o ZrO_2 (2.5 v/o Y_2O_3) composite from 550 MPa (80,000 psi) to 930 MPa (135,000 psi). Decreasing the size of the hard agglomerates through sedimentation (supported under Rockwell IR&D) further increases the strength to 1035 MPa (150,000 psi). At this strength level, unusual shaped voids left by organic matter (lint) are observed at fracture origins. During this contract year, a new process has been developed to eliminate the void space produced by organic matter which further increases the average strength to 1300 MPa (190,000 psi). One specimen (not included in this average) did not fail after exceeding the load cell limit by 10%. The tensile stress on this specimen exceeded 2000 MPa (300,000 psi).

During the second contract year, systematic investigation has concentrated on 1) the stresses that arise during differential shrinkage due to differential initial bulk density (i.e., those stresses that produce the strength degrading crack-like voids), and 2) the control of grain growth with second phases (large grains are fracture origins).

As detailed in Appendix II, the stresses arising due to differential shrinkage were determined experimentally. Results showed (to our surprise) that the maximum stress arises during the early stages of sintering. Stress relaxation experiments showed that despite the lower differential strain and strain rate during the early stage of sintering, the composite was much more elastic, leading to the development of larger stresses. At high temperatures, the relaxation times are very short and, thus, stresses can quickly relax to zero. These results have major implications in sintering agglomerated powders, powders with differential compositions (e.g., multilayered capacitors), and sintered powder/fiber composites by pointing a direction to minimize sintering stresses and eliminating crack-like void formation produced by differential shrinkage.

As detailed in Appendix III, large grains are fracture origins and must be eliminated to increase strength. Use of a second phase (SiC in Al_2O_3) to limit grain growth and increase strength (by 60%) has been demonstrated (Appendix I). Theory shows that despite large residual stresses developed during cooling due to differential thermal contraction, inclusions will not produce strength degrading microcracks if their size is less than a critical size. Thus, inclusions can be incorporated into ceramic microstructures to limit grain size without introducing strength degrading microcracks. The grain growth studies detailed in Appendix III were carried out with different Al_2O_3/ZrO_2 composites. The principal conclusion of this work was that grain growth control (avoidance of exaggerated grains) could be achieved, providing all (or most) of the four-grain junctions contained an inclusion that hindered grain growth. This condition depends on the size and volume fraction of the inclusion phase, and on the uniformity with which the inclusion phase is distributed. This work has strong implications on engineering the grain size of a material to maximize the potential strength of sintered ceramics.

During the current (third) contract year, systematic effort was concentrated in three areas: 1) the elimination of voids produced by organic inclusion, viz. one important processing related flaw populations, 2) a fea-

sibility study using energy dispersive x-ray spectra to quantify the uniformity of phase distribution in multiphase ceramics, and 3) the effects of attrition milling, which introduces impurities on the fabrication, microstructure and properties of transformation toughened ZrO_2.

As detailed in Appendix IV, organic inclusions (e.g., lint) produce irregular shaped voids observed at fracture origins. These voids can be eliminated from a powder compact by a presintering processing step: organic burnout at a temperature prior to bulk shrinkage and iso-pressing at room temperature. This procedure was demonstrated for the case of voids produced by polystyrene spheres (4 to 100 μm diameter).

As detailed in Appendix V, a preliminary study was undertaken to determine if EDAX spectra, obtained at different magnifications, might be used to define the phase distribution in a multiphase material. Al_2O_3/ZrO_2 composites were used for the study. EDAX spectra were acquired for a number of arbitrarily selected areas at each magnification using a commercial scanning electron microscope/x-ray detector/multichannel analyzer system. A statistical analysis of the spectra showed that the deviation from the mean phase distribution increased with magnification. These results showed that the smallest area that contained the same phase distribution as the whole specimen could be defined if one first defines an acceptable deviation from the mean. Spectra acquired for the same area suggest that an acceptable deviation is 5% of the mean. Within the limits of multi-element detectability, these preliminary results strongly suggest that this EDAX method could be used as a quality assurance tool throughout the processing and fabrication of a multiphase material.

As detailed in Appendix VI, the effect of attrition milling and post-sintering heat treatment on the fabrication, phase relations, microstructure and properties of ZrO_2 (+ 2.2 v/o Y_2O_3) powder used to produce a transformation toughened material were examined. Powder used to fabricate the unmilled material was treated and consolidated by a colloidal method. The same powder, treated and consolidated by the same method, but ball-milled in a commercial

alumina mill before consolidation, was used to fabricate the milled material. Both materials were sintered at 1400°C/1 h and then heat treated at higher temperatures. Milling introduced Al_2O_3 inclusions (< 1 vol%) and a glass phase (7 to 10 vol%). The milled powder was more difficult to sinter and exhibited more bloating during heat treatment. TEM observations indicated that the larger glass content of the milled material beneficially reduced residual stresses due to thermal contraction anisotropy. A limited Al solid-solubility in the ZrO_2 structure was suspected to cause the milled material to enter the two phase (tetragonal and cubic) field at a lower heat treatment temperature than observed for the unmilled material.

Upon entering the two-phase region, large (presumably cubic) grains heterogeneously nucleated to produce a bimodal grain size distribution which was more pronounced on the surface of the heat treated, milled materials. Large pores produced during heat treatment in the two-phase field were coordinated by larger grains. It is hypothesized that the pores were produced by the release of high pressure oxygen during phase decomposition ($t \rightarrow t' + c$).

Both fracture toughness (K_c) and hardness of dense, as-sintered materials were unaffected by milling (contamination with Al_2O_3 and glass). Hardness decreased with bloating and the decrease was more pronounced for the milled material. The tetragonal to monoclinic transformation was spontaneous in both materials after heat treating in air at 250°C/16 h. This unwanted transformation phenomena was not observed in vacuum, suggesting it is caused by a reactant present in air.

LIST OF PUBLICATIONS RESULTING FROM CURRENT AFOSR PROGRAMS

1. F.F. Lange, "Processing Related Fracture Origins: Part 1, Observations in Sintered and HIP Treated Al_2O_3/ZrO_2," J. Am. Ceram. Soc. 66, 396 (1983).

2. F.F. Lange and M. Metcalf, "Processing Related Fracture Origins: Part 2, Agglomerate Motion and Crack-Like Internal Surface Produced by Differential Sintering," J. Am. Ceram. Soc. 66, 398 (1983).

3. F.F. Lange, I.A. Aksay and B.I. Davis, "Processing Related Fracture Origins: Part 3, Differential Sintering of ZrO_2 Agglomerates in Al_2O_3/ZrO_2 Composites," J. Am. Ceram. Soc. 66, 407 (1983).

4. F.F. Lange, "Formation of Crack-Like Voids and Agglomerate Motion due to Differential Sintering," 5th CIMTEC (in press).

5. B. Kellett and F.F. Lange, "Stresses Induced by Differential Sintering in Powder Compacts," J. Am. Ceram. Soc. (in press, May 1984).

6. F.F. Lange and N. Claussen, "Some Processing Requirements for Transformation Toughened Ceramics," Proc. Conf. on Ceramic Ultrastructures, University of Florida, Gainsville, Feb. 1983 (AFORS-sponsored), in press.

7. F.F. Lange and M. Hirlinger, "Hindrance of Grain Growth in Al_2O_3 by ZrO_2 Inclusions," J. Am. Ceram. Soc. 67, 164 (1984).

8. F.F. Lange, "Structural Ceramics: A Question of Fabrication," ASM Conf. on Materials for Future Energy Systems, to be published by ASM.

9. F.F. Lange, B.I. Davis and E. Wright, "Processing Related Fracture Origins IV: Eliminating Voids Produced by Organic Inclusions," to be published in J. Am. Ceram. Soc.

10. F.F. Lange and M.M. Hirlinger, "Phase Distribution Studies using Energy Dispersive X-Ray Spectra Analysis," to be published.

11. F.F. Lange, H. Shubert, N. Claussen and M. Ruhle, "Effects of Attrition Milling and Post-Sintering Heat Treatment on Fabrication, Microstructure and Properties of Transformation Toughened ZrO_2," to be published in J. Mat. Sci.

PROGRAM'S CONTRIBUTION TO STUDENT DEVELOPMENT

Two university students were supported under the current AFOSR program: Mr. Bruce Kellett, a graduate student in the Materials Engineering Department at UCLA, took part in the program to determine the sintering stresses due to different sintering (see Appendix II). This work is his M.S. thesis topic. He has been accepted to go on for his Ph.D. Dr. F.F. Lange, an Adjunct Professor at UCLA, is his advisor.

Miss Margaret Hirlinger, an undergraduate student in the Physics Department at MIT, took part in the grain growth studies (see Appendix III) during the summer of 1982 and the EDAX study (see Appendix V) during the summer of 1983. She is an outstanding young student who we are encouraging to continue her expertise in Materials Science. She will be working with us again this summer.

APPENDIX I

Structural Ceramics: A Question of Fabrication Reliability

F. F. Lange

Rockwell International Science Center
Thousand Oaks, California 91360

ABSTRACT

Structural ceramics based on silicon nitride, silicon carbide and transformation toughened zirconium oxide are potential candidates for advanced heat engines. Flaw populations, introduced during processing, currently limit their reliability. Processing steps responsible for common flaw populations will be discussed. It will be shown that new processing steps, based on colloidal powder treatments, combined with second phase engineering can increase fabrication reliability.

CERAMIC HEAT ENGINES have been under study and testing for more than 20 years. Earnest work in the United States on advanced gas turbines initiated in the late 60's at Ford with the use of reaction-bonded silicon nitride (Si_3N_4) for critical components such as combustion chambers and stator vanes, and at Westinghouse in 1968 with hot-pressed Si_3N_4, first commercialized in the U.S. by Norton, for the testing of stator vanes in huge powder generating turbines. This U.S. work reinitiated programs in Britain, where both reaction-bonded and hot-pressed Si_3N_4 were invented, and initiated heat engines and structural ceramic programs in Germany, Japan, Sweden, France, Italy, China, and more than likely, the Soviet Union. In the late 70's, emphasis was shifted from gas turbines to adiabatic diesels with less stringent requirements (lower temperatures, lower stresses, fewer components, etc.) and greater apparent payoff.

The cyclic temperature operation of heat engines and the nonductile (nonstress relieving) behavior of ceramics over a wide temperature range requires that candidate ceramics be chosen to best minimize thermal stresses, viz. ceramics with low thermal expansion, low elastic modulus, high strength and high thermal conductivity. The size of the component and surface heat exchange rates, which are dictated by component design and operation, also govern thermal stresses. Today, candidates which best meet these property requirements at temperatures > 800°C are ceramics based on either silicon nitride (Si_3N_4) or silicon carbide (SiC). Since both require second phase additions to fabricate dense shapes from powders, both are polyphase, polycrystalline materials.

Properties, particularly those of Si_3N_4, depend on the choice of the densification aid which, combined with impurities, govern the chemistry and content of the second phases. The attributes of each material class (Si_3N_4 vs SiC) depends on the application. Si_3N_4 has a smaller thermal expansion coefficient ($\alpha_{Si_3N_4} = 3 \times 10^{-6}/°C$ vs $\alpha_{SiC} = 4.2 \times 10^{-6}/°C$), a smaller elastic modulus ($E_{Si_3N_4} = 300$ GPa vs $E_{SiC} = 420$ GPa) which better minimize thermal stress for extreme conditions, and a higher potential for strength due to its larger fracture toughness ($K_{c(Si_3N_4)} = 4$ to 6 MPa$\cdot m^{1/2}$ vs $K_{c(SiC)} = 3$ to 4 MPa$\cdot m^{1/2}$). SiC, on the other hand, has a much higher thermal conductivity which can better minimize thermal stresses for less severe conditions (smaller or thin walled components and low surface heat exchange rate coefficients), and does not exhibit significant property degradation until much higher (> 1500°C) temperatures relative to Si_3N_4 (> 1250°C). For these reasons, critical gas turbine components (vanes, rotors, combustors, etc.) used for testing are manufactured from either Si_3N_4 or SiC. Low expanding, glass-ceramic compositions are used for lower temperature components (flow path containment, heat exchangers, etc.).

The need for low thermal conducting materials for current adiabatic diesel designs is in direct conflict with candidate materials

which best minimize thermal stresses. The thermal conductivity of current Si_3N_4 and SiC materials is equal or greater than that for case iron. Here, zirconium dioxide (ZrO_2), which is an exceptionally poor thermal conductor, is emerging as a prime candidate, despite the fact that its thermal expansion is ~ 3 times that of Si_3N_4, and therefore develops greater thermal stresses The ZrO_2 materials under investigation take advantage of a relatively new phenomenon called transformation toughening that results in high fracture toughness (K_c = 6 to 12 $MPa \cdot m^{1/2}$ at room temperature) and therefore high potential strengths.

Ceramic heat engine programs have produced many positive results. Design engineers, who have been forced to work with materials engineers due to the lack of formal education in brittle material design, have discovered new design concepts to minimize stress concentration within comonents and contact stresses between components which have led to failure. Full ceramic engines have run for short periods at temperatures where metal engines would not survive. Individual components have survived for extended periods. Material scientists have developed relations between fabrication, composition, microstructure and properties which have led to improved materials and less costly fabrication methods. Although improved designs and materials are still needed for commercial realization of ceramic heat engines, the current major problem resides with the unpredictable strength of the ceramic itself, leading to the unpredictable failure of similar components tested under similar conditions.

It is widely acknowledged that the unreliable structured behavior of ceramic components and specimens is due to the large variation of pre-existing flaw types and sizes. Strength (σ) is proportional to the material's fracture toughness (resistance to crack extension) as measured by the critical stress factor, K_c, and the size (c) of the largest pre-existing crack (or flaw):

$$\sigma \propto \frac{K_c}{\sqrt{c}} \quad .$$

Experimental and analytical methods based on Weibull statistics have been developed in an attempt to treat the 'unpredicatable' strength of ceramics.[1] These methods involve an analysis of fracture data to obtain statistical parameters which characterize the material's failure probability. These statistical parameters are used to design components under known loads, and thus stress distributions to obtain exceptable survival probabilities. Unfortunately, inconsistent fabrication procedures result in large variations in the 'characteristic' statistical parameters, viz. parameters obtained from one batch of material may not characterize the next batch.

Overload proof testing procedures and analysis that incorporate time dependent strength phenomena have also been developed to insure component survival.[2] These tests are not only costly, but may not mimic operating stress distributions with sufficient accuracy to insure survival under real, operating conditions. Programs aimed to develop nondestructive evaluation methods to identify the small, strength limiting flaws in ceramics have not made sufficient progress to be used in the foreseeable future for either accepting or rejecting ceramic components.

The ceramics community recognizes that flaw pupulations in virgin ceramic components are in someway related to inhomogeneities introduced during fabrication. All ceramics are fabricated by sintering preformed powder shapes by inducing mass transport at high temperatures to eliminate void space. Flaw populations must be related to inhomogeneities introduced during the different steps in this process, viz. powder manufacture, powder processing, powder consolidation to shape, sintering and subsequent machining. The average size, size distribution and types of inhomogeneity introduced during each fabrication step will determine the average strength and strength distribution. It can be concluded that the poor reliability of current ceramics is primarily due to the unpredictable distribution of inhomogeneities introduced during fabrication. Namely, the structural reliability of ceramics is a problem of fabrication reliability.

Identification of the fabrication steps producing strength degrading inhomogeneities and the changes in fabrication, and/or microstructure required to eliminate the inhomogeneities (or reduce their size) is critical to improving the structural reliability of ceramics. Such a program has been initiated at Rockwell's Science Center. Different flaw populations, observed at fracture origins, have been related to inhomogeneities introduced by different processing steps. New fabrication procedures have been identified which either eliminate or reduce the size of the inhomogeneities, and therefore their corresponding flaw populations. These new fabrication procedures not only lead to higher strengths, but also uncover the next flaw population to be tackled by innovative fabrication procedures.

The following sections will summarize five common flaw populations (crack-like voids produced by agglomerates, voids left by organic matter, inclusions, large grains and surface cracks), how they are introduced during fabrication, and new fabrication methods of minimizing their effect on potential strength.

CRACK-LIKE VOIDS PRODUCED BY AGGLOMERATES[3] - Agglomerates are common to all powder processing routes. They can be classified as either soft, i.e., particles held together by Van der Walls forces which can be broken apart with surfactants, or hard, i.e., partially sintered groups of particles which require attrition to dismember. All dry powders contain soft agglomerates. Hard agglomerates are common to powder manufacturing routes that involve heating to decompose an oxide precursor. Some processing routes (spray drying) purposely form large agglomerates to produce a flowable 'powder' for dry pressing.

It has been shown that agglomerates are retained when powders are consolidated to the desired shape prior to sintering. During sintering, the agglomerate can shrink differently from one another and/or their surrounding powder matrice. The differential shrinkage of the agglomerate relative to its surrounding matrix can produce a crack-like void. The crack-like void can either extend radially from the agglomerate for the case where the matrix undergoes a greater shrinkage, or extend circumferentially for the case where the agglomerate undergoes greater shrinkage. Figure 1 illustrates an example of a circumferential crack-like void produced by the greater shrinkage of a ZrO_2 hard agglomerate in a two phase, transformation toughened Al_2O_3/ZrO_2 matrix.

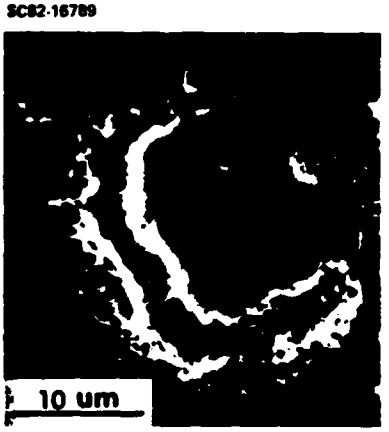

Fig. 1 - Circumferential crack-like void produced during sintring by a ZrO_2 hard agglomerate in a Al_2O_3/ZrO_2 composite.

The crack-like voids can be eliminated (or reduced in size) by two methods. First, the crack-like voids present in the near theoretically dense (> 98%) bodies can be closed by hot gas isostatic pressing (HIPing). HIP treatment can significantly increase the strength of a Al_2O_3/ZrO_2 sintered body (500 MPa for sintered to 875 MPa for sintered and HIP'ed).

The second approach is more fundamental to processing science.[4] It involves dispersing the powder(s) in a liquid containing a surfactant which eliminates the soft agglomerates and consolidating the powder from the slurry state to form the desired engineering shape, which is dried and sintered. The colloidal route can also be used to obtain uniform dispersions of two or more phases. Hard agglomerates cannot be broken apart with surfactants. The colloidal route can still be used to eliminate hard agglomerates greater than a given size by sedimentation. Using the colloidal route, both single phase transformation toughened (TT), tetragonal ZrO_2 (+2.2 m/o Y_2O_3), and two phase TT Al_2O_3 v/o ZrO_2 (+2.2 m/o Y_2O_3) have been sintered to $> 0.98\ p_t$ to result in a mean strength > 1000 MPa (150,000 psi). Fracture origins in these stronger materials are no longer crack-like voids due to agglomerates, but voids produced by organic contaminants, such as lint.

VOIDS PRODUCED BY ORGANIC INCLUSIONS - Organic inclusions (lint, hair, etc.) are commonly found in powders; clean rooms are ineffective when powders are shipped from the manufacturer containing organic inclusions. Such inclusions pack with the powder during consolidation and leave irregular shaped voids when they burn out during sintering. These irregular shaped voids are found at fracture origins and are therefore a common flaw population. Figure 2 illustrates such an irregular void produced by a cellulose fiber which commonly leaves a residual skeletal ceramic backbond within the void.

Fig. 2 - Long void located at a fracture origin in transformation toughened Al_2O_3/ZrO_2 (30 v/o) produced by the burn-out of lint (organic matter).

One method for eliminating such voids is simply to burn out the organic matter at a low

temperature, cool to room temperature, isopress the powder compact, and then sinter. Iso-pressing after burn-out and before sintering can eliminate the void produced by the organic inclusions and further increase the average strength of transformation toughened ZrO_2 from 1050 MPa (152,000 psi) to 1300 MPa (185,000 psi).

INCLUSIONS[5] - Large, second phase inclusions are commonly observed at fracture origins, as shown in Fig. 3, for the case of a SiC inclusion in dense Si_3N_4. Such inclusion

Fig. 3 - Fracture surface of Si_3N_4 (Norton, NC132) showing frature origin (a) and SiC inclusion (b) at fracture origin.

are usually contaminates introduced during powder manufacture and processing. Since the thermal expansion and/or elastic properties of the inclusion are different than the matrix phase, localized stresses develop within and around the inclusion during cooling from the fabrication temperature and/or during subsequent stressing. The distribution of these stresses are well known for simple inclusion shapes, viz. spheres and ellipsoids. The largest tensile stress arises at the inclusion/matrix interface. For the case of differential thermal contraction, the magnitude of the largest tensile stress depends on the elastic properties of the two phases, the change in temperature, and which of the two phases contacts more during cooling.

When certain conditions are met, a small preexisting flaw at the inclusion/matrix interface can extend into a large microcrack, either during cooling or subsequent stressing. Similar to the agglomerate problem discussed above, the type of microcrack developed depends on whether the inclusion contracts more than the matrix (circumferential) or less than the matrix (radial). Although analyses of this problem have produced many subtle and interesting conclusions, the major conclusion is that the conditions for microcrack formation not only depends on the magnitude of the maximum tensile stress and the size of the preexisting flaw, but also on the size of the inclusion. That is, for a given maximum residual tensile stress (σ_r) microcracks will not form during cooling if the inclusion is less than a critical size, R_c^o.

Analyses concerning the effect of an added, applied tensile stress are more recent. Again, the principal conclusion is that the inclusion size also governs the formation of a microcrack under residual and applied tensile stresses. That is, if the inclusion is too small to produce a microcrack during cooling ($R < R_c^o$), then a microcrack can be produced at an applied stress (σ_a) dependent on the inclusion size:

$$R > R_c = R_c^o \, F\left(\frac{\sigma_a}{\sigma_r}\right) \quad ,$$

where the function $F(\sigma_a/\sigma_r)$ is ≤ 1 and depends on the type of crack (e.g., circumferential or radial).

These results are important to the fabricator who must guard against strength degrading inclusions. The results tell the fabricator that despite the possibility of large residual stresses, inclusions will not produce any strength degradation at a given applied stress if their size is $< R_c$. Here again, colloidal dispersion and sedimentation can be used to eliminate inclusions greater than a given size.

The above results are also important to those who would want to design new materials for new properties by producing composites of two (or more) compatible phases (e.g., to achieve a desired thermal expansion, etc.). That is, despite large differences in thermal and mechanical properties, two-phase composites can have mechanical integrity if the size of the second phase is less than a critical value.

CONTROL OF GRAIN SIZE - Bimodel and large grain size microstructures must be avoided to obtain high strengths. Large single grains within a fine grain matrix are common fracture origins. It is also well known that average strength is inversely proportional to the average grain size. Similar to the case of inclusions discussed above, localized stresses arise within and around grains due to thermal expansion and elastic anisotropy. The conditions for microcracking in single phase polycrystalline ceramics are similar to those of inclusions. That is, a critical grain size exists for spontaneous microcracking during cooling. Spontaneous microcracking occurs in single phase, polycrystalline Al_2O_3 with an average grain size > 80 μm. For materials exhibiting a much greater thermal expansion anisotropy, e.g., $MgTi_2O_5$[6] and Nb_2O_3,[7] the critical grain size is < 5 μm. Similar to the inclusion case, an applied stress will reduce

the critical grain size required for spontaneous microcracking. Control of grain growth is therefore required for mechanical integrity.

It is well known that control of grain growth can be achieved with the addition of a chemically compatible second phase. As discussed in the previous section, two phase composites can be designed to avoid microcracking. Figure 4 illustrates the strengthening that can be achieved for Al_2O_3 with

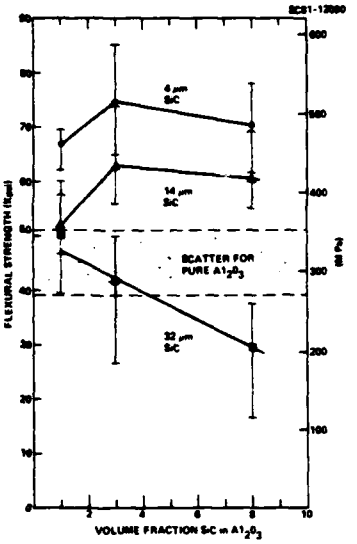

Fig. 4 - Flexural strength of Al_2O_3/SiC composites vs volume fraction and size of SiC particulates.

additions of SiC with an average particle size of 4 μm.[8] Despite the large differential thermal expansion ($\alpha_{Al_2O_3} = 8 \times 10^{-6}/°C$, $\alpha_{SiC} = 4.2 \times 10^{-6}/°C$), small additions (1 v/o to 8 v/o) of the 4 μm SiC can decrease the average grain size from ~ 30 μm to ~ 5 μm to increase the average strength by a factor of 1.6.

Recent results[9] indicate that the second phase is most effective when located at four-grain junctions, viz. it costs more energy to relocate the inclusion within a grain from a four-grain junction than a two-grain junction. Grain growth of the major phase will therefore be controlled by the number of four-grain junctions filled by the second phase. Thus the second phase size distribution, volume fraction and uniformity of distribution are critical parameters. Figure 5 illustrates the average Al_2O_3 grain size and the largest to average size ratio in various Al_2O_3/ZrO_2 composites as a function of temperature. At higher temperatures, grain growth control

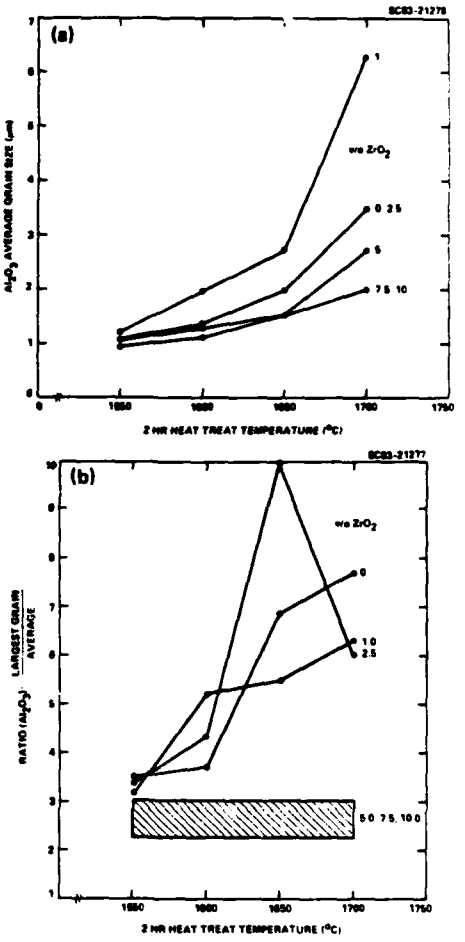

Fig. 5 - Al_2O_3 average grain size (a) and ratio of largest to average size (b) for a series of Al_2O_3/ZrO_2 composites vs heat treatment temperatures (2 hrs).

required ZrO_2 volume fractions > 0.075 for the given sizes distribution of starting powders. Note that 1 v/o ZrO_2 produces a much larger grain sizes relative to pure Al_2O_3. This result is caused by the nonuniformity of the ZrO_2 distribution, i.e., some portions of the material contained a higher concentration of ZrO_2 than others.

It should be noted here that when colloid routes are employed to achieve a uniform phase distribution, the fabricator must guard against sedimentation. Figure 6 illustrates bottom and top regions of a slip cast β''-Al_2O_3/15 v/o ZrO_2 composite. The large ZrO_2 agglomerates and large β''-Al_2O_3 grains sedimented to the bottom. This problem can be avoided by pre-sedimentation as discussed above and/or by flocking the colloid prior to consolidation.

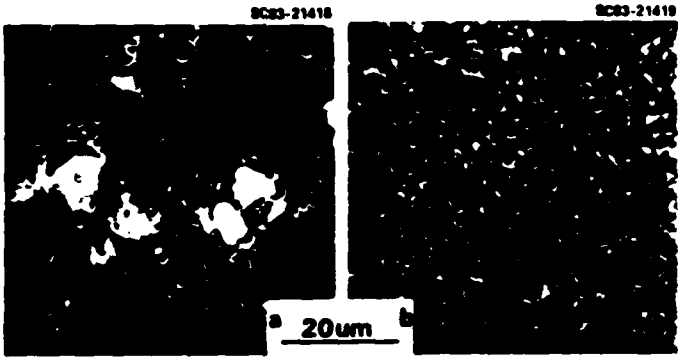

Fig. 6 - Bottom (a) and top (b) regions of a slipcast β"-Al_2O_3/ZrO_2 composite powder compact after sintering. Note large single phase areas on bottom due to sedimentation (courtesy of D.J. Green).

It can be concluded that the mechanical reliability of a ceramic can be increased by controlling grain growth with a dispersed second phase. This approach can be optimized with strict controls on phase distribution.

SURFACE CRACKS - Final shaping of ceramic components is performed by diamond grinding, a process that unavoidably introduces surface cracks. Rice et al[10] have shown that two type of radial cracks exist within the groove made by the plowing abrasive grain: 1) closely spaced cracks that traverse the groove produced by *slip-stick, and* 2) longitudinal cracks which overlap one another along the length of the groove. The overlapping, longitudinal cracks produce the greatest strength degradation and result in a strength anisotropy when tensile strength is measured parallel and perpendicular to the grinding direction.

It has been demonstrated that the effect of surface cracks on strength degradation can be minimized by the introduction of residual surface compressive stresses. The most effective means of introducing residual surface compressive stresses is by inducing a molar volume increase at the surface through either a stress induced phase transformation or a chemical reaction.

Abrasive machining or particle impact of transformation toughened ZrO_2 materials induces the tetragonal to monoclinic ZrO_2 transformation at the surface. The molar volume increase (~ 3%) that accompanies this transformation can produce compressive surface stresses as high as 1000 MPa (150,000 psi).[11] Contrary to other classes of ceramics, the strength of transformation toughened ceramics is significantly increased <u>after</u> abrasive grinding.

Molar volume increases can also be induced at the surface by a chemical reaction with the environment, e.g., oxidation.[12] Here, a two phase ceramic is engineered such that the second phase increases its volume through a surface reaction. As demonstrated, for the Si_3N_4/Zr-oxynitride system, the magnitude of the surface compressive stresses depends on the volume fraction of the second phase Zr-oxynitride, the molar volume increase produced by the Zr-oxynitride + $O_2 \rightarrow ZrO_2 + N_2$ reaction, and the depth of the reaction layer which is governed by oxidation kinetics (temperature and time). If the volume fraction of the Zr-oxynitride phase is > 0.10, the compressive surface stresses can be too severe and will eventually produce surface spalling.

CONCLUDING REMARKS - It has been demonstrated that strength limiting flaw population, inherent to conventional ceramic fabrication procedures, can be eliminated or minimized using new fabrication methods and by engineering two phase materials. Voids produced by the differential shrinkage of agglomerates and/or organic inclusions can be eliminated by post-sintering HIP (hot gas isopressing) treatments, a process that the ceramic manufacturers are beginning to implement. A more cost effective approach is the use of colloidal methods for powder treatment and consolidation.

Colloidal methods (powder dispersion, sedimentation and slurry consolidation) effectively reduces the size of agglomerates and inclusions. They also uniformly distribute second phases needed to control abnormal grain growth and/or to produce residual surface compressive stresses through environmental reactions. Effort to further develop these colloidal methods will certainly increase the fabrication and structural reliability of ceramics.

ACKNOWLEDGEMENTS - Work at the Science Center uncovering processing related flaws in

ceramics is supported by the Air Force Office or Scientific Research under Contract No. F49620-81-C-0036.

REFERENCES

1. Wiederhorn, S.M., "A Probabilistic Framework for Structural Design," Fracture Mech. of Ceramics, Vol. 5, p. 97, eds., R.C. Bradt, A.G. Evans, D.P.H. Hasselman and F.F. Lange, Plenum Press (1983).

2. Ritter, Jr., J.E. "Assessment of Reliability of Ceramic Materials," ibid p. 227.

3. Lange, F.F., M. Metcalf, B.I. Davis and I.A. Aksay, "Processing-Related Fracture Origins: Parts I, II and III," J. Am. Ceram. Soc. 66, 396-408 (1983).

4. Lange, F.F. and B.I. Davis, "Sinterability of ZrO_2 and Al_2O_3 Powders: The Role of Pore Coordination Number Distribution," Zirconia '83 (Stuttgart, June 1983), Conf. Proc. in press with Am. Ceram. Soc.

5. Green, D.J. "Microcracking Mechanisms in Ceramics," ibid, Ref. 1, p. 457.

6. Kuszyk, J.A. and R.C. Bradt, J. Am. Ceram. Soc. 56, 420 (1973).

7. Manning, W.R., O. Hunter, Jr., F.W. Calderwood and D.W. Stacy, J. Am. Ceram. Soc. 55, 342 (1972).

8. Lange, F.F., unpublished data.

9. Lange, F.F. and M.M. Hirlinger, "Hindrance of Grain Growth in Al_2O_3 by ZrO_2 Inclusions," J. Am. Ceram. Soc. 67, 164 (1984).

10. Rice, R.W., J.J. Mecholsky, Jr. and P.F. Becker, "Effect of Grinding Direction on Flow Character and Strength of Single Crystal and Polycrystalline Ceramics," J. Mat. Sci. 16, 853 (1981).

11. Green, D.J., F.F. Lange and M.R. James, "Factors Influencing Residual Stresses Due to a Stress-Induced Phase Transformation," J. Am. Ceram. Soc. 66, 623 (1983).

12. Lange, F.F., "Compressive Surface Stresses Developed in Ceramics by an Oxidation-Induced Phase Change," J. Am. Ceram. Soc. 63, 38 (1980).

Rockwell International
Science Center

Stresses Induced by Differential Sintering in Powder Compacts

BRUCE KELLETT*

Department of Materials Science and Engineering, School of Engineering and Applied Science, University of California, Los Angeles, California 90024

F. F. LANGE*

Rockwell International Science Center, Thousand Oaks, California 91360

Stresses created by differential sintering, due to differences in initial bulk density, were determined, to an order of magnitude, by an experiment which estimated the differential sintering phenomenon on a macroscopic level. The experiments entailed determining the shrinkage rates of a powder isostatically pressed to two bulk densities. Using this information, stresses were determined by forcing the slower-densifying compact to shrink at the same rate as the faster-densifying compact and measuring the resulting forces with a load cell. Maximum stresses (between 1 and 3 MPa) were observed to occur in the intermediate stage of densification. Despite larger differential strains at higher temperatures, stresses decreased to zero at the latter stage of densification. Viscoelastic experiments, of the stress-relaxation type, were performed. Results showed that the sintering specimen was more rigid at lower temperatures and more fluidlike at higher temperatures. This explains the development of maximum stresses at intermediate temperatures.

I. Introduction

THE processing of ceramics is currently the focus of much attention. Based on recent work in the area of fracture mechanics, researchers now feel that great improvements in the fracture strength of ceramics are possible with improved processing. These improvements hinge on the ability of the ceramist to eliminate flaw populations inherent to certain processing methods. Agglomerates produced a major flaw population by causing cracklike voids to form by differential sintering.[1,2] In this case, agglomerates produce inhomogeneous density distributions which can carry through to the sintered body as cracklike voids.

Sintering kinetics are dependent on many variables, like green density, composition, particle size, and morphology. Therefore any green body, which is inhomogeneous, will show differences in shrinkage strains from one region to the next (Fig. 1). The corresponding differential strains between these regions are expected to give rise to stresses within the powder compact during sintering.

Any calculation used to determine these stresses would have to consider microscopic details of the inhomogeneities and the local shrinkage behavior of the powder compact. In addition, the stress/strain behavior of the powder compact during the period of densification would need to be known. We attacked this problem on a more tractable macroscopic level. We considered the powder compact to be inhomogeneous only with regard to green density. In particular, we chose a commonly realized inhomogeneity within powder compacts, namely a higher-density agglomerate surrounded by a powder matrix of lower density. To determine the maximum stress produced by this arrangement, the shrinkage rates of powder compacts of two bulk densities were measured at constant heating rates. The slower-densifying compact was then forced to densify at the same rate as the faster-densifying compact within a mechanical test machine that measured the resulting force. In this manner, the stress arising from differential sintering was determined over the full range of heating with only one assumption concerning the stress-strain behavior of the densifying powder compact, viz., both the low and high bulk density compacts exhibit similar viscoelastic behavior.

II. Experimental Procedure

A composite powder consisting of 70 vol% Al_2O_3* and 30 vol% ZrO_2† was used for this study. An equivalent of 2 mol% Y_2O_3 was added to the ZrO_2 as $Y(NO_3)_3$.‡ The material was ball-milled in methanol with high-alumina balls in a polyethylene container overnight, flash-evaporated, and then calcined at 600°C overnight to convert the $Y(NO_3)_3$ to Y_2O_3. The composite powder was ground with a mortar and pestle, and then axially pressed (28 MPa) into cylindrical specimens (2.54 by 0.847 cm). The cylindrical compacts were isostatically pressed at 69 and 345 MPa to produce specimens with densities of 2.22 and 2.63 g/cm^3, respectively.

The compacts were sintered in air and shrinkage measurements for both the high and low bulk density compacts were obtained for heating rates of 5°, 10°, and 20°C/min (between 900° and 1550°C) using an extensometer described elsewhere.[3] Results, expressed as dimensionless strain ($\varepsilon = \Delta l/l_0$), were obtained with three or more specimens for each bulk density and for each heating rate

*ALCOA A16 superground, Aluminum Company of America, Pittsburgh, PA
†Zircar Div., Union Carbide Corp., Niagara Falls, NY
‡Research Chemical Div., Nucor Corp., Phoenix, AZ

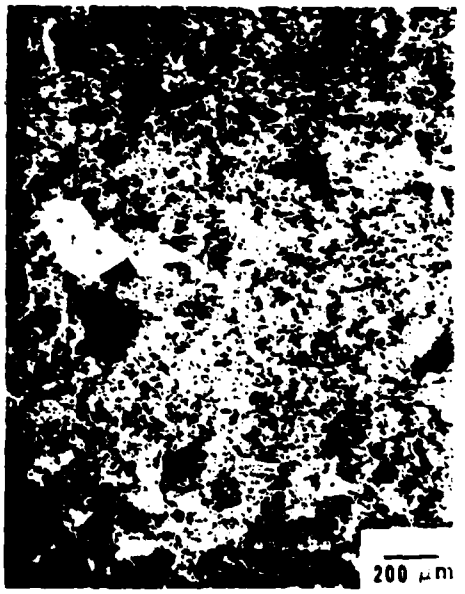

Fig. 1. Density variations produced by isopressing of dry aluminum-zirconia composite powder (sintered to ≈90% of theoretical density).

Presented at the 35th Pacific Coast Regional Meeting, The American Ceramic Society, Seattle, Washington, October 28, 1982 (Paper No. 21-B-82P). Received July 15, 1983, revised copy received October 3, 1983, approved January 26, 1984.
Supported by the Air Force Office of Scientific Research under Contract No. F49620-81-C-0036.
*Member, the American Ceramic Society.

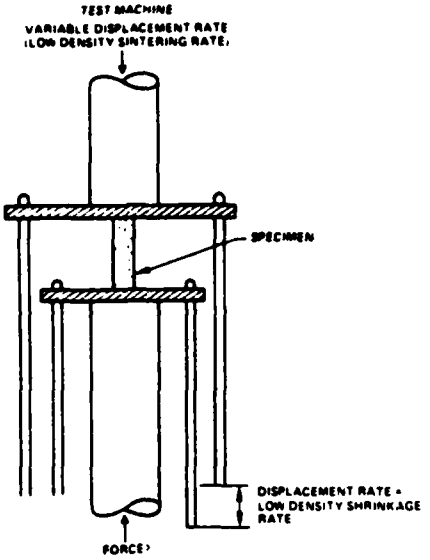

Fig. 2. Schematic of loading train and extensometer used to force specimen with higher green density to sinter at same rate as that with lower green density.

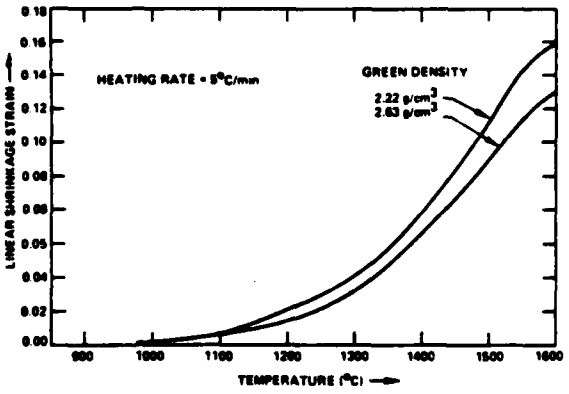

Fig. 3. Shrinkage strain vs temperature for Al_2O_3-30 vol% ZrO_2 powders with different initial bulk densities (2.22 and 2.63 g/cm³) heated at 5°C/min.

To determine the sintering stresses, a high green density specimen was placed in a furnace between SiC rods attached to the moving crosshead of a mechanical testing machine.[8] During heating the crosshead was moved to mimic the displacement rate of the lower green density compact. The thermal expansions of the load train had to be experimentally determined and subtracted from the applied displacement rate. These expansions were experimentally determined for the two heating rates (5° and 10°C/min) used to determine stresses. This was accomplished by bringing the two ends of the load train together and determining the displacement rate required to maintain a constant applied load on the load train during heating at the desired heating rate.

Each constant heating rate experiment was initiated at 900°C. A displacement rate was applied to the specimen which forced it to shrink (uniaxially) at the same rate as the lower green density compact. This displacement rate was determined for each heating

[8]Instron Corp., Canton, MA.

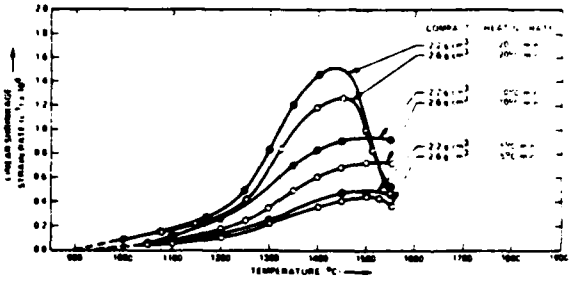

Fig. 4. Shrinkage strain rate vs temperature for compacts with high and low green densities heated at three heating rates.

rate by subtracting the expansion history of the loading train from the shrinkage history determined by experiments described above. An extensometer (see Fig. 2) was used to ensure that the correct displacements were applied.

Viscoelastic experiments of the stress-relaxation type were performed to determine the changing nature of the sintering body with temperature. These experiments required the same apparatus as described above for the sintering-stress experiments. The tests were performed at T = 1000° to 1550°C using a high green density specimen which was sequentially tested from low to high temperature. The relaxation experiments entailed quickly applying a small compressional strain to the specimen to obtain an initial stress between 1 and 7 MPa, depending on temperature. The initial stress was allowed to dissipate at constant strain. Since these tests caused only a slight compressional strain, negligible densification occurred. The powder compact was modeled as a Maxwell element[3] with the spring acting as the compact's elastic skeleton and the dash pot corresponding to its viscous processes (sintering and deformation). The characteristic relaxation time λ was determined from the time taken for the stress to decay to $1/e$ of its initial value. The characteristic relaxation time is a measure of the compact's viscosity to elastic modulus ratio (η/E).

III. Results

As shown by the example in Fig. 3 (heating rate = 5°C/min), the lower green density compact always showed greater shrinkage strains than the higher green density compact. Shrinkage at all heating rates initiated at ≈1000°C. Differential shrinkage between the high- and low-density compacts was sufficiently significant to be observed beginning at about 1050°C.

Shrinkage rates were determined graphically as a function of temperature. As shown in Fig. 4, the shrinkage rate which peaked at high temperature (>1450°C), was greater for faster heating rates, and for the low-density compact relative to the higher-density compact for a given heating rate. The differential shrinkage rate between the two density compacts was the greatest at 1550°, 1500°, and 1435°C for heating rates of 5, 10, and 20°C/min, respectively. Conversion of the linear shrinkage data into density ($\rho = \rho_0/(1-\varepsilon)^3$, where ρ_0 is the initial green density) showed that the higher green density compact was always more dense than the low-density compact despite its lower shrinkage rate, as shown in Fig. 5.

Experiments to determine the stress produced by differential shrinkage were performed at heating rates of 5° and 10°C/min. Figure 6 illustrates these data. Although the form of the data was consistent from one specimen to the next, individual experiments produced different stresses. The data scatter between experiments was caused by slight, but consistent, deviations in the applied crosshead displacement rates relative to the displacement rates which exactly mimic the shrinkage rate of the low-density compact. For this reason, the maximum stress could only be estimated as ranging between 1 and 3 MPa and no differences could be observed for the two heating rates. As shown in Fig. 6, the stresses

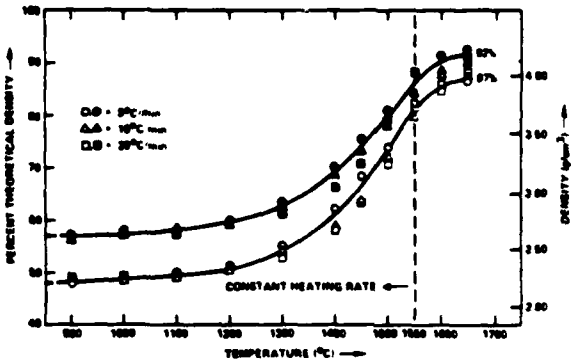

Fig. 5. Relative density vs temperature for high- and low-green-density Al_2O_3-30 vol% ZrO_2 compacts sintered at three heating rates.

increase to a maximum value at ≈1200°C and then dissipate to approximately zero at 1500°C.

Results of stress-relaxation experiments are shown in Fig. 7. As illustrated, the characteristic relaxation time decreased by about three orders of magnitude between 1000° and 1500°C. At $T > 1400$°C, data were difficult to obtain since the stresses relaxed nearly as fast as they were applied. Thus, in general, the viscoelastic compact can be described as an elastic body at low temperatures and a viscous body at high temperatures.

IV. Discussion

For this experiment the lower green density compacts exhibit a greater shrinkage and shrinkage rate over that of the high green density compact. As demonstrated here, the differential shrinking produced by a green-density differential of ≈0.4 g/cm³ (2.22 g/cm³ vs 2.63 g/cm³) results in maximum stresses ranging between 1 and 3 MPa for the heating rates studied. Although the maximum differential strain and differential strain rates occurred at high temperatures (>1450°C), the maximum stress occurred at relatively low temperatures (≈1200°C). Stress-relaxation experiments strongly suggest that the maximum stress arises at lower temperatures because the material is more elastic, whereas stresses dissipate at high temperatures due to easier diffusion.

Since the densifying powder compact exhibits viscoelastic behavior over its complete range of densification (see Fig. 7), one would expect that the magnitude of the stresses would be proportional to the strain rate which, as shown in Fig. 4, is proportional to the heating rate. That is, the maximum stress developed due to differential sintering might be minimized by heating at a slower rate over the critical temperature range (≈1200°C for the case examined here). Unfortunately, the accuracy of the current experiments did not permit any correlation between heating rate and maximum stress.

One might ask: Is 1 to 3 MPa sufficient to produce the cracklike voids observed by the differential sintering of agglomerate/matrix systems? The answer is beyond the scope of the present work, but it might be pointed out that, in model studies, the cracklike voids were observed to form during the initial stage of sintering where the powder compact is expected to be weakest.[4]

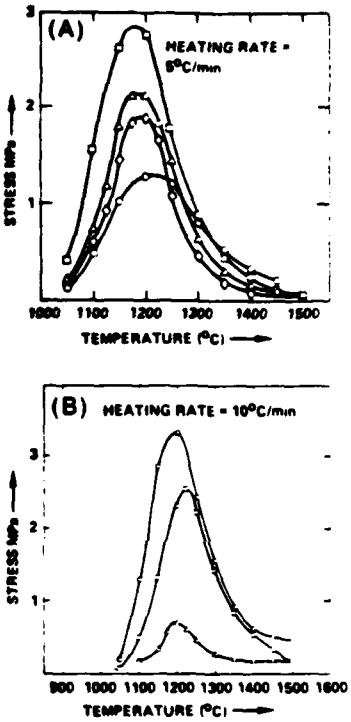

Fig. 6. Stresses resulting from forcing high-green-density compact to shrink at same rate as lower-green-density compact at heating rates of (*A*) 5°C/min and (*B*) 10°C/min. different data points represent different runs

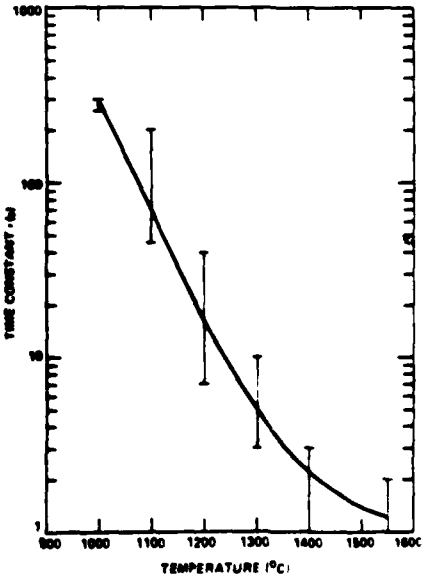

Fig. 7. Characteristic relaxation time constant vs temperature

References

[1] K. D. Reeve, "Non-Uniform Shrinkage in Sintering," *Am. Ceram. Soc. Bull.*, 42 [8] 452 (1963).
[2] F. F. Lange, "Processing-Related Fracture Origins: I. Observations in Sintered and Isostatically Hot-Pressed Al_2O_3/ZrO_2 Composites," *J. Am. Ceram. Soc.*, 66 [6] 396–98 (1983).
[3] F. F. Lange, B. I. Davis, and D. R. Clarke, "Compressive Creep of Si_3N_4/MgO Alloys: I. Effect of Composition," *J. Mater. Sci.*, 15 [3] 601–10 (1980).
[4] F. F. Lange and M. Metcalf, "Processing-Related Fracture Origins: II. Agglomerate Motion and Cracklike Internal Surfaces Caused by Differential Sintering," *J. Am. Ceram. Soc.*, 66 [6] 398–406 (1983).

Rockwell International
Science Center

Reprinted from the Journal of the American Ceramic Society, Vol. 67, No. 3, March 1984

Hindrance of Grain Growth in Al_2O_3 by ZrO_2 Inclusions

F. F. LANGE* and MARGARET M. HIRLINGER

Structural Ceramics, Rockwell International Science Center, Thousand Oaks, California 91360

APPENDIX III

Alumina and Al_2O_3/ZrO_2 (1 to 10 vol%) composite powders were mixed and consolidated by a colloidal method, sintered to >98% theoretical density at 1550°C, and subsequently heat-treated at temperatures up to 1700°C for grain-size measurements. Within the temperature range studied, the ZrO_2 inclusions exhibited sufficient self-diffusion to move with the Al_2O_3 4-grain junctions during grain growth. Growth of the ZrO_2 inclusions occurred by coalescence. The inclusions exerted a dragging force at the 4-grain junctions to limit grain growth. Abnormal grain growth occurred when the inclusion distribution was not sufficiently uniform to hinder the growth of all Al_2O_3 grains. This condition was observed for compositions containing ≤2.5 vol% ZrO_2, where the inclusions did not fill all 4-grain junctions. Exaggerated grains consumed both neighboring grains and ZrO_2 inclusions. Grain-growth control (no abnormal grain growth) was achieved when a majority (or all) 4-grain junctions contained a ZrO_2 inclusion, viz., for compositions containing ≥5 vol% ZrO_2. For this condition, the grain size was inversely proportional to the volume fraction of the inclusions. Since the ZrO_2 inclusions mimic voids in all ways except that they do not disappear, it is hypothesized that abnormal grain growth in single-phase materials is a result of a nonuniform distribution of voids during the last stage of sintering.

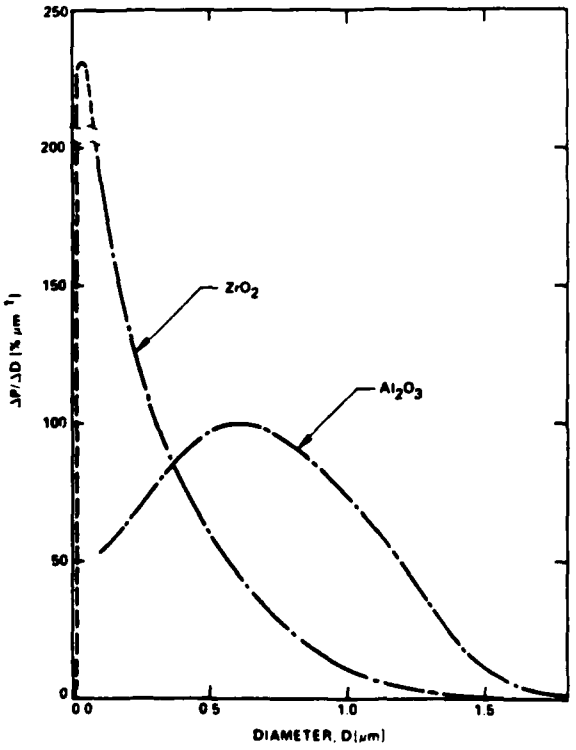

Fig. 1. Size distribution of colloidally treated Al_2O_3 and ZrO_2 powders (distribution for sizes <0.1 μm was not determined and is given by dashed line).

I. Introduction

GRAIN-GROWTH inhibition is desirable for preventing abnormal grain growth during sintering, which allows pores to be swallowed to limit end-point densities, and for limiting grain size to achieve higher strengths.* Second-phase inclusions can inhibit grain growth and are frequently used for this purpose in metal systems. Although most high-performance ceramics are not single-phase materials, the use of a particular second phase to inhibit grain growth is not currently practiced due to the common belief that inclusions are precursors to strength-degrading microcracks. Although inclusions can produce microcracks, theoretical work has shown that, despite the high residual stresses developed by differential thermal expansion (or phase changes), microcracking can be avoided both during cooling from the fabrication temperature and during subsequent stressing if the inclusion size is less than a critical value.[1,2] This theoretical work has opened the possibility of designing two (or more) phase systems without the worry of degrading strength and other properties related to microcracking, as was recently demonstrated for Al_2O_3/SiC composites.[3] Despite the large differential in thermal expansion (the thermal expansion of Al_2O_3 is twice that of SiC), an SiC-dispersed phase inhibits grain growth to produce a 65% strength increase relative to polycrystalline Al_2O_3 fabricated under identical conditions.

Theory that treats the inhibition of grain growth by inclusions has generally been based on refinements of Zener's[4] original concept, in which the inclusion residing at the grain boundary produces a dragging force due to the lower free energy of the junction/inclusion system when the inclusion resides at the junction. Ashby and Centamore[5] showed that the inclusion(s) can move with the junction if the inclusion exhibits sufficient self-diffusion. Theory suggests that the velocity of the moving inclusion (v_i) will depend on its radius r as either r^{-3} or r^{-4}, for interfacial diffusion or volume diffusion, respectively.[6]

In metal systems, inclusions are commonly introduced by precipitation, internal oxidation, mechanical alloying, etc., and they are usually used to control grain growth during the recrystallization that precedes deformation at temperatures where the inclusion's velocity is nearly zero. These methods of introducing inclusions into ceramics are ineffective since grain-growth inhibition must be concurrent with sintering. Thus, inclusions must be introduced as a second-phase particulate dispersion into the major-phase powder prior to sintering. Since detailed studies of inclusion/grain-junction interactions have not been detailed for this method of fabrication, studies were initiated by investigating the effect of ZrO_2 additions on the grain-growth phenomena of Al_2O_3. This system was chosen for the large difference in atomic number between Al and Zr, which results in high contrast between the two chemically compatible phases when examined by electron microscopy. Green[7] has already characterized grain growth to determine the critical ZrO_2 inclusion size required to retain the tetragonal structure. Since powders of both phases can be sintered within the same temperature range (1300° to 1600°C), it was suspected that sufficient self-diffusion would exist within the ZrO_2 to permit analogies with pore/grain boundary interactions.

Received July 12, 1983; revised copy received December 15, 1983; approved December 27, 1983.
Supported by the Air Force Office of Scientific Research under Contract No. F49620-81-C-0036.
*Member, the American Ceramic Society.
*Each grain can be considered a precursor to a microcrack due to either residual stresses arising from thermal expansion anisotropy or effects of surface machining.

Table I. Grain-Size Data for Al_2O_3 and Al_2O_3/ZrO_2 Composites

ZrO_2 content (vol%)	Grain size parameter*	Heat-treatment temperature/time (°C/h)						
		1550/2	1600/2	1650/2	1650/6	1650/12	1700/2	1700/2†
0	A	1.09	1.36	1.95			3.52	3.74
	AR	3.5	3.7	6.9			7.7	4.0
1	A	1.21	1.98	2.69	3.74	5.28	6.30	11.50
	Z	0.54	0.55					
	AR	3.2	5.2	5.5	6.4	6.4	6.3	3.5
	Z/A	0.45	0.27					
2.5	A	1.05	1.31	2.04			3.48	
	Z	0.44	0.54					
	AR	3.4	4.4	10.0			6.0	
	Z/A	0.41	0.41					
5	A	1.05	1.23	1.49	1.98	2.48	2.75	
	Z	0.52	0.58	0.65	0.84	0.96	1.32	
	AR	2.66	2.92	2.82	3.13	3.50	2.76	
	Z/A	0.37	0.47	0.43	0.42	0.39	0.48	
7.5	A	0.95	1.32	1.57	1.73	1.95	2.01	2.08
	Z	0.51	0.72	0.93	0.89	0.94	1.19	
	AR	2.75	3.03	2.48	2.54	2.90	2.69	3.17
	Z/A	0.54	0.54	0.59	0.52	0.48	0.59	
10	A	0.91	1.09	1.48	1.51	1.91	1.90	
	Z	0.57	0.74	0.98	0.97	1.21	1.20	
	AR	3.07	3.02	2.84	2.78	3.03	2.21	
	Z/A	0.63	0.68	0.66	0.64	0.63	0.63	

*A = Al_2O_3 mean size (μm), Z = ZrO_2 mean size (μm), AR = largest Al_2O_3 grain/mean size; Z/A = mean ZrO_2/mean Al_2O_3. †Specimens heated directly to 1700°C for 2 h

II. Experimental Procedure

Alpha Al_2O_3 and cubic ZrO_2 (+6.6 mol% Y_2O_3) powders were separately dispersed in distilled water containing HCl to maintain a pH of 2 to 3 for up to 24 h.* Each powder was sedimented to collect all particles ≤1 μm. The supernatant containing ≤1 μm particles was immediately flocced by increasing the pH to 8 with additions of NH_4OH. Flocculation consolidated the dispersion to ≈16 and ≈5 vol% for the sedimented Al_2O_3 and ZrO_2 powders, respectively, and prevented mass segregation during storage. The small salt content resulting from pH controls was minimized by mixing the flocced slurries with deionized water, followed by spontaneous flocing. The solid contents of each flocced slurry were determined by density measurements and the assumed density of each phase ($\rho_{Al_2O_3}$ = 3.98 g/cm³, ρ_{ZrO_2} (cubic) = 6.03 g/cm³). Figure 1 illustrates the size distribution of the two powders after they were redispersed at pH = 2, diluted to ≈2 vol%, and ultrasonically treated.

Two-phase flocced slurries containing 0, 1.0, 2.5, 5.0, 7.5, and 10.0 vol% ZrO_2 were prepared by weighing the appropriate amounts of each slurry, redispersing each at pH = 2 with HCl, mixing together with ultrasonic treatment, and again flocing at pH = 8 with NH_4OH. As described elsewhere, consolidation was performed by centrifuging at ≈2000 times gravity. The centrifuged, plastic mass was dried and cut into specimens and sintered together at 1550°C for 1 h.† All materials had a sintered density ≥97% of theoretical based on the theoretical densities of the two phases.

Each material was diamond-cut into a smaller specimen and one surface was highly polished. Thermal etching was performed at 1550°C for 1 h. Polished, thermally etched surfaces were observed in the scanning electron microscope using a combined backscattering and secondary electron-collecting mode to enhance the contrast between the two phases required to measure the size distribution of the brighter ZrO_2 inclusions.

A number (4 to 8) of micrographs were taken at a magnification for which every Al_2O_3 grain could be analyzed with an image analyzer. The size distribution of the Al_2O_3 grains was obtained by tracing the grain boundaries on the micrographs with black ink on a transparent overlay suitable for image analyzing. The image analyzer was programmed to convert each phase area into an equivalent circle to obtain its equivalent diameter. These data were reduced to a histogram and pertinent statistical parameters. The same specimens were then heat-treated for 2 h at 1600°, 1650°, and 1700°C. Specimens containing 1, 5, 7.5, and 10 vol% ZrO_2 were also heat-treated at 1650°C for 2, 6, and 12 h prior to the 1700°C heat treatment. After each heat treatment, the size distributions of both the ZrO_2 and Al_2O_3 grains were obtained by the same procedure discussed above. The number of grains observed for each phase was dependent on the volume fraction of the ZrO_2 and the development of a bimodal distribution for the Al_2O_3. Different magnifications were used for bimodal microstructures. In addition, separate specimens containing 1 and 7.5 vol% ZrO_2 were directly sintered at 1700°C for 2 h without the intermediate heat treatments.

*Initial reaction tended to increase the pH, which decreased the stability of the dispersion.

†Initial sintering experiments showed that a sintering temperature of 1525°C (1 h) produced densities ≤95% of theoretical.

III. Results

(1) Grain-Growth Data

Table I lists the statistical information reported as mean grain size of the Al_2O_3 (A) and ZrO_2 (Z), mean size ratio of the two phases (Z/A), and the largest-to-mean size ratio of the Al_2O_3 phase (AR). Values of AR indicated the bimodal nature of the microstructure. The determination of AR was somewhat subjective for extreme bimodal microstructures since it was uncertain that the largest grain was photographed during examination. Figure 2 illustrates the mean grain size of the Al_2O_3 (*A*) and the largest-to-mean ratio (*B*) as a function of the 2-h heat-treatment temperatures.

Figure 2(*A*) shows that the mean Al_2O_3 grain size is not a monotonic function of the ZrO_2 content, viz., the grain sizes for composites with 1 and 2.5 vol% ZrO_2 were greater than and equal to that for the single-phase Al_2O_3, respectively. Figure 2(*B*) shows that all of the materials containing ≤2.5 vol% were strongly bimodal at ≥1600°C, whereas grain-growth control (normal grain growth) was achieved for ZrO_2 contents ≥5 vol%.

Table I shows that the mean size of the ZrO_2 inclusions at 1550°C is larger than the mean size in the initial ZrO_2 powder and that they continue to grow during heat treatments at T>1550°C. In general, their size after a given heat treatment increases with ZrO_2 volume fraction.

For composites exhibiting controlled grain growth (≥5 vol% ZrO_2) the mean size ratio of the two phases (Z/A) was nearly constant at all temperatures and increased with the ZrO_2 volume fraction (see Table I).

Journal of the American Ceramic Society—Lange and Hirlinger Vol. 67, No. 3

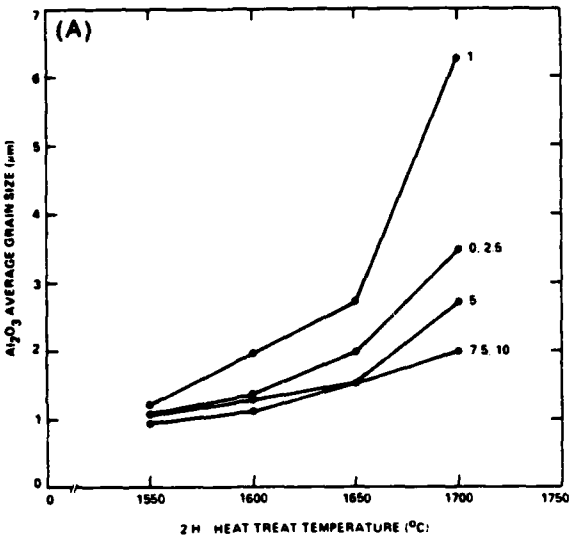

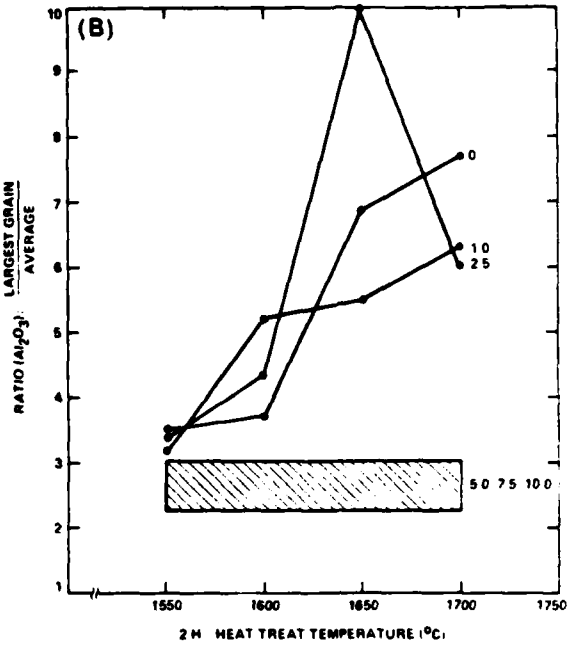

Fig. 2. Temperature of 2-h heat treatment vs (*A*) mean Al_2O_3 grain size and (*B*) ratio of largest Al_2O_3 grain size to mean grain size (numbers on curves represent vol% ZrO_2).

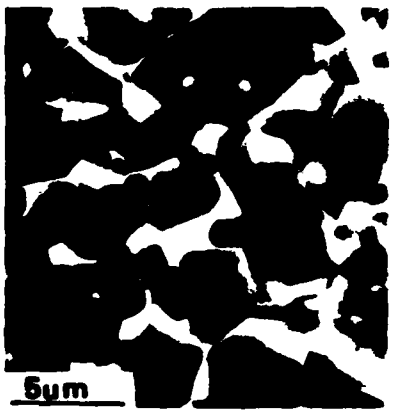

Fig. 3. Fracture surface of 7.5 vol% ZrO_2 composition after heat treatment at 1700°C for 2 h; most ZrO_2 inclusions lie at 4-grain junctions.

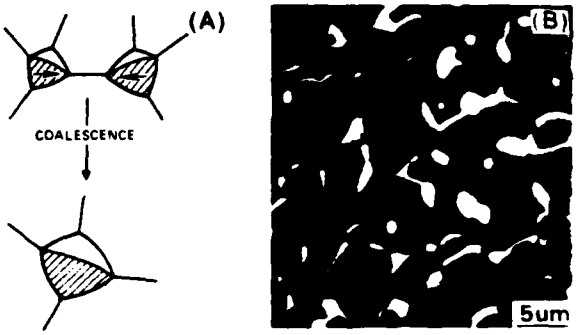

Fig. 4. (*A*) Diagram showing coalescence of inclusions at 4-grain junctions and (*B*) micrograph showing several ZrO_2 grains at 4-grain junctions resulting from coalescence (5 vol% ZrO_2, 1700°C for 2 h).

Direct heating of the 7.5 vol% ZrO_2 composition to 1700°C/2 h produced a nearly identical microstructure to the same material sintered at 1550° and sequentially heated to 1700°C (see Table I). This was not the case for the Al_2O_3 without a dispersed phase and the 1 vol% ZrO_2 composition. Direct heating to 1700°C/2 h produced larger grains without the severe bimodal characteristics of the same materials heated sequentially to 1700°C. These observations suggest that the conditions for exaggerated grain growth are history-dependent and may reflect a nucleation/growth phenomenon for abnormal grain growth.

(2) Microstructures

For composites exhibiting controlled grain growth (≥5 vol% ZrO_2), fracture-surface observations showed that the ZrO_2 grains were primarily located at 4-grain junctions,[6] as illustrated in Fig. 3 for the case of 7.5 vol% ZrO_2 heated to 1700°C/2 h. It is obvious that ZrO_2 particles, initially located between the Al_2O_3 particles, were sufficiently mobile during growth of the Al_2O_3 grains to remain located at 4-grain junctions. That is, the growth of the ZrO_2 grains occurred by coalescence, as depicted in Fig. 4(*A*); Fig. 4(*B*) illustrates that ZrO_2/ZrO_2 grain boundaries were frequently observed, indicating a coalescence mode of growth.

For compositions that produced a bimodal Al_2O_3 grain-size distribution (≤2.5 vol% ZrO_2), the ZrO_2 grains were primarily located at 4-grain junctions[6] only at 1550°C. At 1550°C, not all 4-grain junctions were filled in the 2.5 vol% composite and relatively few were filled in the 1 vol% composite. At higher temperatures, more and more ZrO_2 grains became relocated within the interior of the Al_2O_3 grains and had a spherical geometry. This phenomenon appeared to occur by the growth of a group of Al_2O_3 grains, constrained by relatively few ZrO_2 grains, into a large grain which then swallowed up surrounding Al_2O_3 and ZrO_2 grains. As shown in Fig. 5, the Al_2O_3 grains in regions with a greater local concentration of ZrO_2 remained small until they were engulfed by much larger, surrounding grains. That is, abnormal grain growth appeared to be promoted when either all 4-grain junctions were not

[6]Surface observations used to determine grain size limit observations to apparent 3-grain junctions.

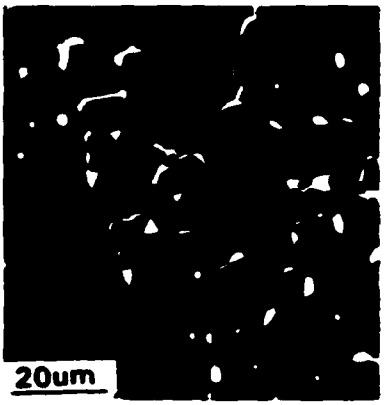

Fig. 5. Region of small Al_2O_3 grains constrained by ZrO_2 inclusion surrounded by large, exaggerated grains. Note arrowhead shape of inclusions at 3- (or 4-) grain junctions (1 vol% ZrO_2, 1700°C for 2 h).

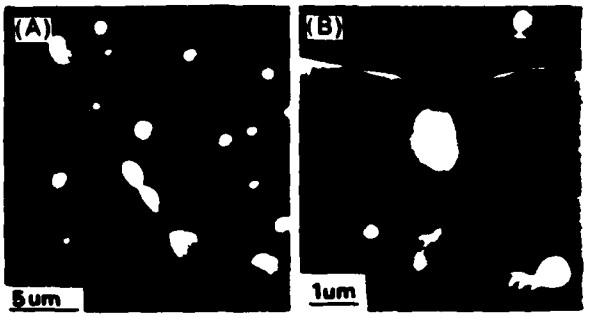

Fig. 6. (*A*) Drag configuration of ZrO_2 inclusions at 2-grain junction and (*B*) imminent breakaway configuration.

filled and/or the inclusion phase was not uniformly distributed.

Within regions containing only abnormally large Al_2O_3 grains, the ZrO_2 grains were more than 10 times smaller than the Al_2O_3 grains. At 2-grain junctions the ZrO_2 grains were observed in various drag/breakaway configurations, as shown in Fig. 6(*A*); Fig. 6(*B*) shows the rare configuration of imminent breakaway. Measurement of the dihedral angle (ϕ) with symmetric ZrO_2 grains located at 2-grain junctions resulted in $\phi = 80° \pm 5°$. This suggests that the Al_2O_3/ZrO_2 interfacial energy is $\approx 2/3$ the Al_2O_3 grain-boundary energy.

The arrowhead shape of ZrO_2 grains at 3-grain junctions (or, possibly 4-grain junctions) also indicates a condition of inclusion drag as recently pointed out by Hsueh *et al.*[8] and Spears and Evans[9] for the case of a pore being dragged by a 3-grain junction (Fig. 7(*A*)). Examples of these shapes are shown in Fig. 5. Figure 7(*B*) schematically shows three configurations observed for an inclusion close to a 3-grain junction. These shapes suggest that the inclusion has recently broken away from the 3-grain junction, by either the movement of two grain boundaries (configuration 1) or by the movement of any one of the grain boundaries (configurations 2 and 3).

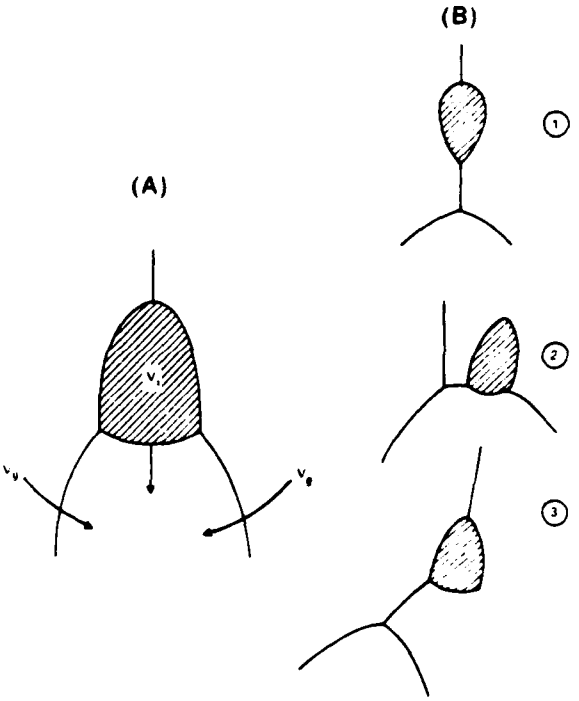

Fig. 7. Schematics showing (*A*) arrowhead shape of inclusion being dragged along with 3-grain junction (after Refs. 8 and 9) and (*B*) observed breakaway configurations.

IV. Discussion

(1) Grain-Growth Control

Grain-growth data and direct observations indicate that the self-diffusion of ZrO_2 was sufficient at all temperatures to allow the ZrO_2 particles, initially located between the Al_2O_3 particles, to locate and remain at 4-grain junctions when grains grew in a controlled manner during sintering and subsequent heat treatments. When abnormal grain growth did not occur ($T \leq 1550°$ and $\geq 1600°C$ for composites containing ≥ 5 vol% ZrO_2), the ZrO_2 inclusions had a relatively minor effect on average grain size; viz., at 1550°C, 10 vol% ZrO_2 reduced the average size of the Al_2O_3 grains by only ≈10%. At higher temperatures, the difference in average grain size for the 5 and 10 vol% ZrO_2 compositions (realm of normal grain growth) was 50%. Evans and co-workers[8,9] showed that the grain-growth hindrance exerted by pores located at 3-grain junctions is directly proportional to the pore-size/grain-size ratio. The same theoretical arguments also apply to 4-grain junctions. Inclusions that exhibit sufficient self-diffusion will behave as pores. Table I shows that, based on the analogy between pores and inclusions, the average grain size decreases as the inclusion size-to-grain size ratio (Z/A) increases.

The major effect of the ZrO_2 inclusions was in preventing abnormal grain growth at temperatures where the inherent resistance of the single-phase material to this phenomenon had disappeared. As shown above (Table I and Fig. 2(*B*)), the inclusions were effective only at volume fractions ≥ 0.05. Smaller volume fractions could both widen the bimodal Al_2O_3 grain-size distribution and increase the average Al_2O_3 grain size. Observations (Fig. 5) suggest that abnormal grains developed from a small group of grains that contained fewer ZrO_2 inclusions and are therefore less inhibited from growing relative to surrounding grains. Once such a group grows to a large grain, it rapidly swallows neighboring grains and inclusions. This is supported by the observations that not all 4-grain junctions were filled for the 2.5 vol% ZrO_2 composite and fewer yet were filled for the 1 vol% composite. These observations strongly suggest that all 4-grain junctions must be filled to uniformly hinder all grains from growing abnormally.[*]

[*]This may be one limiting case. Bimodal microstructures could also be prevented if the inclusions were uniformly distributed such that, although not all 4-grain junctions were filled, viz., the nuclei for abnormal growth (i.e., groups of grains unhindered by inclusions) were small and uniformly dispersed. This would require a *uniform dispersion of inclusion, a task that, in practice,* would be more difficult to achieve than filling all 4-grain junctions.

As detailed in the appendix, filling all 4-grain junctions requires a critical volume fraction (V_c) of the inclusion phase. V_c depends on the average size ratio of the major-phase and inclusion-phase powders and on factors that govern the clustering of the inclusion phase during powder mixing.

Observations further suggest that abnormal grain growth is promoted when the inclusions do not fill all 4-grain junctions and are not uniformly distributed, causing uninhibited groups to act as nuclei for potential, abnormal grains.

(2) *Analogies to Pore/Grain-Size Phenomena*

If the dominating path of ZrO_2 diffusion is at the ZrO_2/Al_2O_3 interface, theory indicates that inclusions will mimic the behavior of pores in all ways except one, viz., pores can disappear by mass transport (i.e., the phenomenon of sintering), whereas inclusion cannot. Analogies between pores and inclusions were presented above concerning drag and breakaway configurations. Of greater interest here are the analogies concerning pore-volume change and grain growth, and conditions leading to abnormal grain growth.

Recent observations[10] showed that sintering is not a homogeneous process, viz., small regions reach full density prior to the bulk. These dense regions support grain growth. The pores separating the dense regions prevent abnormal grain growth, i.e., grain growth is confined to the dense regions. As these pores shrink and disappear, one can classify the pore/grain-growth phenomenon with two extreme cases. The first case is where grains grow and pores coalesce. In this case, pore disappearance will prevail until the pores offer little hindrance to grain growth. The exact pore fraction at which this occurs will depend on how uniformly the pores are distributed. Kingery and Francois[11] suggested that this phenomenon can certainly occur when the pore-volume fraction is ≈0.10. In this case, the pores located at 4-grain junctions are dragged with the junction to maintain a uniform but magnified microstructure where the pore size-to-grain size ratio remains constant due to pore coalescence at newly formed 4-grain junctions in the same manner observed for the ZrO_2 inclusion in the present study.

In the second extreme case, i.e., the case where pores disappear faster than grains grow, grain growth will be initially restricted to dense regions, as discussed above. When the pore volume decreases to some critical volume fraction, the distribution of porosity will now govern the condition for grain growth as for the inclusion case. If this distribution is inhomogeneous, some dense regions will enlarge. Grain growth in these dense regions will result in much larger grains than in regions where grain growth is still hindered by porosity. This condition sets the stage for abnormal grain growth, i.e., grains within the dense regions grow rapidly to swallow neighboring grains and pores. Results presented for the ZrO_2 inclusions suggest that an inhomogeneous pore distribution can result in exaggerated grain growth for a volume fraction less than a critical value, e.g., $V_c \leq 0.05$. Thus, it might be concluded that exaggerated grain growth is promoted by the nonuniform distribution of pores (or inclusions). Agglomerates that densify prior to the bulk are therefore prime candidates and sites for exaggerated grain growth.

APPENDIX

Filling Four-Grain Junctions with Inclusions

Let us assume that the average grain in a single-phase polycrystal can be represented by a polyhedron with n_0 vertices and that this average configuration is unchanged during normal grain growth. Since each vertex is shared by four grains, $n_0/4$ inclusions are needed to fill all 4-grain junctions per grain. The powder used to fabricate the polycrystal has an average particle diameter D_m. We now introduce a second-phase powder with an average particle diameter D_i such that either single particles or particle clusters will form as inclusions located at the 4-grain junctions, i.e., positions of lowest free energy. We assume that during normal grain growth, the inclusions remain at 4-grain junctions to grow by coalescence such that the size ratio of the two-phase entities (viz., clusters particles or inclusion grains) remains constant throughout sintering and subsequent normal grain growth. If the average number of second-phase particles in a cluster is n_c, then the volume fraction of second-phase particles (V_c) required to just fill all 4-grain junctions is

$$V_c = \frac{\frac{n_0}{4} n_c \frac{\pi}{6} D_i^3}{\frac{n_0}{4} n_c \frac{\pi}{6} D_i^3 + \frac{\pi}{6} D_m^3} \tag{A-1}$$

which can be rearranged to

$$V_c = \frac{1}{1 + \frac{4}{n_0 n_c}\left(\frac{D_m}{D_i}\right)^3} \tag{A-2}$$

The degree of clustering, represented by n_c above, will depend on how well the two powders are mixed and on how many second-phase particles would fit in the interstices formed by the packing of the major-phase particles, i.e., n_c might be expected to increase with D_m/D_i. That is, the probability of clustering will increase with D_m/D_i, i.e., V_c will be expected to be a weak function of D_m/D_i above a given value of D_m/D_i. For example, if the major-phase particles were monodispersed spheres, packed together with a face-centered-cubic arrangement, more than one second-phase particle could fill an octrahedral interstice when $D_m/D_i > 5$. Since powder-packing arrangements usually produce larger interstices relative to the octrahedral site in the fcc arrangement, one might consider $D_m/D_i = 5$ as an upper limit to avoid high probabilities of clustering and therefore redundant additions of second-phase particles to fill all 4-grain junctions.**

Using Eq. (A-2), values of V_c were calculated for two average grain configurations: (1) the Kelvin, tetrakaidecahedra (14-sided, $n_0 = 26$) used to fill space and achieve grain boundaries with net zero curvature and (2) the 12-sided polyhedron ($n_0 = 14$) formed by deforming spheres with an fcc arrangement, a configuration commonly used to represent average grains in a polycrystal. Using $n_c = 1$ and $D_m/D_i = 5$, $V_c = 0.049$ and 0.027 for these two configurations, respectively, consistent with a value of 0.05 reported above for controlled grain growth.

Acknowledgments: The authors thank D. J. Green, P. E. D. Morgan, and I. Aksay for helpful discussions.

References

[1]F. F. Lange, "Fracture Mechanics and Microstructural Design", pp. 799–820 in *Fracture Mechanics of Ceramics, Vol. 4*. Edited by R. C. Bradt, D. P. H. Hasselman and F. F. Lange. Plenum, New York, 1978.
[2]D. J. Green, "Microcracking Mechanisms in Ceramics", pp. 457–78 in *Fracture Mechanics of Ceramics, Vol. 5*. Edited by R. C. Bradt, A. G. Evans, D. P. H. Hasselman, and F. F. Lange. Plenum, New York, 1983.
[3]F. F. Lange and A. Arora, "Microcracking Phenomena and Strength of Al_2O_3 SiC Composites"; unpublished work.
[4]C. Zener, quoted by C. S. Smith, *Trans. Met. Soc. AIME*, 175, 15 (1949).
[5]M. F. Ashby and R. M. A. Centamore, "The Dragging of Small Oxide Particles by Migrating Grain Boundaries in Copper," *Acta. Met.*, 16 [9] 1081 (1968).
[6]P. G. Shewman, "Movement of Small Inclusions in Solids by a Temperature Gradient," *Trans. Met. Soc. AIME*, 230 [6] 1134 (1964).
[7]D. J. Green, "Critical Microstructures for Microcracking in Al_2O_3/ZrO_2 Composites," *J. Am. Ceram. Soc.*, 65 [12] 610–14 (1982).
[8]C. H. Hsueh, A. G. Evans, and R. C. Coble, "Microstructural Development During Final/Intermediate Stage Sintering-I Pore/Grain Boundary Separation," *Acta Met.*, 30 [7] 1269 (1982).
[9]M. A. Spears and A. G. Evans, "Ibid. II-Grain and Pore Coarsening," *Acta Met.* 30 [7] 1281 (1982).
[10]F. F. Lange, "Sinterability of Agglomerated Powders," *J. Am. Ceram. Soc.* 67 [2] 83–89 (1984).
[11]W. D. Kingery and B. Francois, "Grain Growth in Porous Compacts," *J. Am. Ceram. Soc.*, 48 [10] 546 (1965).

**Note in Table I that the smallest Z/A ratio where controlled grain growth was achieved with additions of ZrO_2 (case of 5 vol% composite) was ≈0.4, which would correspond to $D_m/D_i = 2.5$.

APPENDIX IV

PROCESSING-RELATED FRACTURE ORIGINS: IV. ELIMINATING VOIDS PRODUCED BY ORGANIC INCLUSIONS

F.F. Lange, B.I. Davis and E. Wright
Structural Ceramics
Rockwell International Science Center
Thousand Oaks, CA 91360

ABSTRACT

Organic inclusions (e.g., lint) produce irregular-shaped voids observed at fracture origins. These voids can be eliminated from a powder compact by a presintering processing step: organic burn-out at a temperature prior to bulk shrinkage and iso-pressing at room temperature. This procedure was demonstrated for the case of voids produced by polystyrene spheres (4 to 100 μm diameter).

Introduction

The potential strength of a ceramic is governed by both fracture toughness, i.e., the material's resistance to crack extension as measured by its critical stress intensity factor, K_c, and flaw populations introduced during fabrication. A ceramic with a high K_c only has a potential for higher strength. Each processing step, starting with powder manufacture, has the potential of introducing a strength degrading flaw population. Therefore, the burden of producing an advanced ceramic with reliable high strength rests with the fabricator who must find new and reliable processing methods that eliminate the flaw populations inherent to methods used to fabricate less demanding, traditional ceramics.

Background

Figure 1 schematically illustrates the sequence of flaw populations vs potential strength that has been uncovered during our investigation of certain pressureless sintered, transformation toughened ZrO_2 and Al_2O_3/ZrO_2 ceramics. This particular sequence was discovered chronologically by observing fracture origins, identifying the inhomogeneity at the fracture origin, relating the inhomogeneity to a processing cause, and then eliminating the inhomogeneity through changes in processing. This procedure uncovers the next strength limiting flaw population observed at a higher mean strength. It should be noted that the flaw populations are overlapping, making cause and effect arguments sometimes difficult to identify. Also, processing changes that may eliminate one population (or move it to a much higher mean strength) may introduce a new, more degrading population.

Different sequential flaw populations may be observed, depending on the material system and the starting fabrication method. For the transformation toughened materials used for this study, grinding induces a phase transformation at the surface, resulting in large residual surface compressive stresses[1,2] that effectively move the surface crack population introduced by grinding to a high potential strength relative to more conventional ceramics.

Abnormally large grains, a flaw population common to other ceramics, are not observed in the present materials. The well distributed ZrO_2 grains within the Al_2O_3/ZrO_2 composites prevent the growth of abnormally large Al_2O_3 grains.[3] Abnormal grain growth is not observed for the single phase tetragonal ZrO_2 (+2.3 mole% Y_2O_3) ceramic sintered at 1400°C; at higher temperatures (or greater Y_2O_3 content), abnormal grain growth is prevented by a second cubic ZrO_2 phase.[5]

The sequence of flaw populations, shown in Fig. 1, were initially uncovered using a series of Al_2O_3/ZrO_2 composite powders which were initially milled to break down agglomerates, mixing the two phases, and consolidated prior to sintering by dry pressing. It was determined[5] that large, soft Al_2O_3/ZrO_2 agglomerates present in the dry powders were retained during consolidation. During sintering, the agglomerates shrunk differently relative to their surrounding agglomerates and/or powder matrix to produce large crack-like voids and an average strength of 560 MPa. By treating the same powders with a surfactant (pH control) to break apart the agglomerates and consolidating from the colloidal state by filtration (slip casting), it was shown that the large crack-like voids could be eliminated.[6] This processing change increased the average strength to 930 MPa, and a new flaw population was then discovered.

The new flaw population was smaller crack-like voids produced by ZrO_2 hard agglomerates,[7] i.e., partially sintered agglomerates produced during powder manufacture, that could not be broken apart with a surfactant. Attempts to break down the hard agglomerates by prolonged ball-milling were not acceptable, viz. a few remained to be discovered at occasional fracture origins. Milling also introduced excessive SiO_2 contamination and changed the electrochemistry requirements to achieve a dispersed state.[6] New processing steps were then sought which would be consistent with the need to consolidate from the slurry state.

The flow chart for the new processing steps are illustrated in Fig. 2 for the case of a two phase, e.g., Al_2O_3/ZrO_2 composite. It consists of sep-

arately dispersing each as-received powder, sedimenting to eliminate hard agglomerates > 1 μm, and flocculating to prevent mass segregation during storage. Flocculating also increased the volume fraction of the particulate phase from < 0.02 to between 0.07 and 0.15, depending on the powder characteristics. The flocced slurry has the consistency and rheology of latex paint.

Two-phase mixtures were prepared by first redispersing each phase separately and then mixing the two dispersed phases with the aid of an ultrasonic horn. For the case of the Al_2O_3 and ZrO_2 powders, both could be dispersed at pH ≈ 2 and flocced at pH ≈ 7 to 9, i.e., the two dispersed phases could be mixed without producing a condition of heteroflocculation, analogous to mixing two rare gases.* The two-phase mixture was then reflocced to prevent mass segregation during storage. Consolidation was carried out by slip casting the flocced, two-phase slurry to prevent mass segregation and density gradients experienced when the two-phase mixture was cast in its dispersed state.** After drying, the case Al_2O_3/30 vol% ZrO_2 (+2.3 m/o Y_2O_3) plates were sintered at 1600°C/h. ZrO_2 (+2.5 m/o Y_2O_3) plates were also fabricated with the same method. The dried ZrO_2 plates were sintered at 1400°C/1h. The drying shrinkage for this method can be intolerable for most applications because the volume fraction of solids in the flocced slurry is < 0.15.

Strength measurements of initial Al_2O_3/ZrO_2 material fabricated with the above method showed that simple immersion of the ultrasonic horn into the redispersed slurries was insufficient to insure complete redispersion and two-phase mixing. Figure 3 shows a large globular ZrO_2 agglomerate observed at one fracture origin indicative of poor redispersion from the flocced state. This situation was remedied by passing the redispersed, two-phase slurry

---

* Recent studies have shown that two flocced states can also be mixed under the action of high shear fields.

** Effort to increase the volume content of the dispersed state by evaporation led to the reintroduction of large crack-like voids produced by soft agglomerates when dried slurry on the container's walls would flake off and fall into the slurry.

through a small chamber containing the ultrasonic horn. The average strengths of Al_2O_3/ZrO_2 and ZrO_2 materials fabricated by this method were 1045 MPa and 1030 MPa, respectively.

Failure origins now appeared to be irregularly shaped voids. The serpentine shape, which included a low density skeletal 'backbone'* of some of these voids (shown in Fig. 4) strongly suggested that this flaw population was associated with organic inclusions (e.g., lint). Although lint problems might be avoided with clean room processing, our experience indicates that powders are shipped from manufacturers already contain such organic inclusions. Thus, a new processing method was sought to avoid the voids produced by organic inclusions, consistent with slurry processing required to avoid large crack-like voids produced by the differential sintering of agglomerates.

This new processing step was developed by reasoning that one could burn the organic inclusions out of a dried, consolidated body at a temperature prior to bulk shrinkage. Voids left by the organic inclusions could then be closed by iso-pressing at room temperature.

This processing step was implemented for the single-phase ZrO_2 (+2.3 m/o Y_2O_3) plates fabricated by the colloidal/sedimentation steps discussed above. The bulk density of the dried plates, consolidated by filtration (slip casting), the flocced slurry was 33% of theoretical (ρ_t = 6.07 gm/cm^3). The dried plates were heated to 800°C (bulk densification initiated at ~ 900°C) for 16 h in an air furnace. After cooling, the plates were iso-pressed at 350 MPa, which increased the bulk density to 48% of theoretical and sintered at 1400°C/1 h. With the added step of organic burn-out and iso-pressing prior to sintering, the average flexural strength was increased from 1030 MPa to 1340 MPa. It should be added that one specimen, not included in this average, did not fail when the load cell of the testing

---

* Experience with unpregrating celulose fibers with oxide precursors has shown that a partially sintered skeletal framework can be produced.

machine was exceeded by ~ 10%. Its flexural strength must exceed 2210 MPa (it was retired from active service to avoid the high probabiity of a second test disappointment).

Examination of the new failure origins showed failure initiated at the surface, but no identifiable clue was found to define the exact inhomogeneity that initiated failure. It was presumed that the new flaw population governing potential strength was surface cracks introduced during machining.

The foregoing strength/processing relations are summarized in Table I. The same starting powders and sintering conditions were held constant throughout this study. With the exception of the inhomogeneities removed by improved processing and only evident upon failure, microstructures (viz. grain size and phase distribution) appeared to remain constant as did the critical stress intensity factor, K_c. Although it might be rightly argued that the processing steps taken to uncover different flaw populations which progressively increased mean strength are not currently amenable to economic processing, and that a post-sintering HIP treatment may eliminate most of the different void populations uncovered here, it is evident that new fabrication routes based on colloidal/slurry processing will become economic to fabricate reliable, advanced ceramics.

With this background, an experimental program was undertaken to determine if voids produced by organic burn-out could be eliminated by isopressing, as suggested in the last processing step.

Experimental Procedure

Polystyrene spheres* (~ 1 v/o) of a well-defined size distribution were introduced into a flocced two-phase Al_2O_3 + 10 v/o ZrO_2 (+6.6 m/o Y_2O_3)

* Duke Scientific, Palo Alto, CA 94306

Table I

Average Flexural Strength (MPa) and Strength Range (in brackets) for Different Pressureless Sintered Processing Methods

Material	K_c* ($MPa \cdot m^{1/2}$)	Dry Press	Colloidal Filtration	Sedimentation Filtration	Organic Burn-Out Iso-Press
Al_2O_3/30 v/o ZrO_2 (2.5 m/o Y_2O_3)	6.9	560 (490-590)	895 (825-965)	1045 (955-1160)	----
ZrO_2 (2.3 m/o Y_2O_3)	5.8	---	---	1030** (825-1300)	1340** (1240-1440)†

* Determined by indentation technique (20 Kgm load); Evans and Charles[9] analysis; K_c was independent of processing method.

** Due to the large shrinkage during drying and sintering, specimens were fractured in 3 pt bending (outer span = 2.03 cm). All other specimens fractured in 4 pt bending (outer span = 2.54 cm, inner span 1.27 cm).

† One specimen, not included in average did not fail at a stress of 2210 MPa (load cell capacity exceeded by ~ 10%).

slurry. The polystyrene spheres were chosen as organic inclusions because they produce well-recognized voids after sintering. Different specimens were prepared with different sphere diameters (viz. mean diameters of 4 μm, 10 μm, 25 μm, 50 μm and 100 μm, with standard deviations of < 10%). Previous studies[8] have shown that voids produced by spheres as small as 1 μm, introduced into the same powders used here, shrink during sintering, but do not disappear until the grain size to sphere size ratio is > 1.5.

Both the Al_2O_3 and ZrO_2 powders were separately dispersed in water (pH 2), sedimented to remove particles (and hard agglomerates) > 1 μm, flocced for storage (pH 8), redispersed for mixing, and then coflocced prior to consolidation, as described in the previous section. The polystyrene spheres (~ 1 v/o) were dispersed into the flocced mixture with the aid of an ultrasonic horn; the high viscosity of the flocced mixture prevented the spheres from segregating after mixing. Disc specimens were fabricated by slip

casting the flocced mixture and drying. Specimens were also prepared that did not contain spheres to determine bulk density as a function of iso-pressure.

Specimens from each sphere diameter series were heated to 800°C/16 h, cooled to room temperature, iso-pressed at pressures ranging from 0 to 350 MPa, and then sintered at 1600°C/1 h. The change in bulk density produced by iso-pressing was measured (dimension and weight) on material not sintered. After sintering, the specimens were diamond-ground and polished to reveal the morphology of the voids produced by the organic burn-out/iso-pressing processing step.

Observations

Figure 5 illustrates that iso-pressing to 350 MPa continually increases the relative density of the dried, as-cast compact from 0.42 to 0.67, whereas pressures > 70 MPa are required to increase the bulk density of the compacts heat-treated at 800°C/16 h. Heat treatment at 800°C also limited the bulk density change.

Observations concerning the effect of iso-pressing on pore morphologies are as follows. Surface grinding resulted in grain pull-out which was difficult to completely remove by surface polishing. It was therefore difficult to unambiguously follow the morphology changes of the voids produced by the 4 μm and 10 μm spheres as easily as the larger voids.

Changes in void morphology produced by the 25 μm and 50 μm spheres are typical to those shown in Fig. 6. Up to an iso-pressure of ~ 70 MPa (applied after the 800°C burn-out), the spherical voids remained intact. At pressures > 100 MPa, the deformation produced instabilites causing multiple particle packing units to dislocate at the void interface. With increasing pressure, more packing units dislocate to fill more of the void volume. At intermediate pressures, the void volume is only partially filled, producing what appears to be a low density inclusion after sintering. At the highest pressure (350 MPa), most, but not all, voids had been apparently sufficiently filled to disappear during sintering. Thus, at pressures > 150 MPa, fewer and

fewer voids are observed on the polished, sintered surfaces. It is presumed that the same phemonena occurred for the voids produced by the smaller spheres (4 μm and 10 μm), except less deformation may be required to completely fill the voids.

The phenomena produced by the 100 μm spheres was somewhat different. First, as shown in Fig. 7, radial cracks were produced when the flocced-cast matrix dried and shrank upon the spheres. Such drying cracks were not observed for the smaller spheres. Iso-pressing first initiated crack closure and partial sintering at ~ 70 MPa. Faint traces of partial cracks, as observed by a broken line of pores, were still observed after iso-pressing at 280 MPa. Second, instabilities around the void created by the iso-pressing were not uniform and appeared to cause a 'caved-in' morphology at low pressures (100 to 150 MPa) and resulted in a semi-spherical void at higher pressures (> 200 MPa). Since the size of the 'caved-in' morphology was larger than the original voids, it might be expected that the radial cracks influenced the inhomogeneous powder flow pattern that produced these morphologies.

Discussion

The experimental study has shown that smaller voids produced by organic inclusions can be minimized (or eliminated) by a presintering, burn-out/iso-pressing treatment, as suggested by previous processing/strength relations. Burn-out temperatures < 800°C would be expected to produce similar results while maintaining a powder compact with a lower compliance.

The void/iso-pressing study was also instructive in other ways. First, the heat treatment at ~ 200°C below the temperature where bulk shrinkages initiate, produces sufficient interparticle bonds (i.e., partial sintering without bulk shrinkage) to prevent an increase in bulk density until a pressure > 100 MPa is applied during iso-pressing. This observation is consistent with other observations showing a redistribution of pores prior to bulk shrinkage, which implies that some multiple particle packing units densify at low temperatures.

Second, it was previously suggested that more tightly bound, multiple particle packing units were the first to move when the bulk density of a powder compact was increased by external forces.[10] The void filling process observed here is consistent with this suggestion.

Third, it was noted that only the largest spheres resulted in radial cracks during drying. This situation is directly analogous to the inclusion problem, where differential strains are developed by thermal expansion mismatch. A thermodynamic analysis shows that microcracks will only extend from an inclusion when the size of the inclusion exceeds a critical value.[11] The analysis also applies, in principal, to the case where a drying powder matrix shrinks around a solid, organic inclusion. For the case examined here, critical diameter is > 50 μm. Thus, large organic inclusions can result in large cracks, as shown in Fig. 7, when their size is greater than a critical value. The critical size will be dependent on the amount of drying shrinkage and the viscoelastic properties of the drying powder compact.

Acknowledgement

This work was performed under AFOSR Contract No. F49020-81-C-0036.

REFERENCES

1. R.T. Pascoe and R.C. Garvie, "Surface Strengthening of Transformation Toughened $ZrO_2Al_2O_3$," in Ceramic Microstructures '76, eds., R.M. Fulrath and J.A. Pask, Westview Press, Boulder, CO (1977), pp. 774-84.

2. D.J. Green, F.F. Lange and M.R. James, "Factors Influencing Residual Surface Stresses Due to a Stress-Induced Phase Transformation," J. Am. Ceram. Soc. 66 [9], 623-29 (1983).

3. F.F. Lange and M.M. Hirlinger, "Hindrance of Grain Growth in Al_2O_3 by ZrO_2 Inclusions," J. Am. Ceram. Soc. 67 [3], 164-8 (1984).

4. F.F. Lange, H. Shubert, N. Claussen and M. Ruhle, "Effects of Attrition Milling and Post-Sintering Heat Treatment on the Fabrication, Microstructure and Properties of Transformation Toughened ZrO_2," to be published.

5. F.F. Lange, "Processing Related Fracture Origins: I. Observations in Sintered and Isostatically Hot-Pressed Al_2O_3/ZrO_2 Composites," J. Am. Ceram. Soc. 66 [6], 396-8 (1983).

6. I.A. Aksay, F.F. Lange and B.I. Davis, "Uniformity of Al_2O_3/ZrO_2 Composites by Colloidal Filtration," J. Am. Ceram. Soc. 60 [10], C190-2 (1983).

7. F.F. Lange, B.I. Davis and I.A. Aksay, "Processing Related Fracture Origins: Part III. Differential Sintering of ZrO_2 Agglomerates in Al_2O_3/ZrO_2 Composites," J. Am. Ceram. Soc. 66 [6], 407-8 (1983).

8. B. Kellett and F.F. Lange, unpublished.

9. A.G. Evans and E.A. Charles, "Fracture Toughness Determinations by Indentation," J. Am. Ceram. Soc. 59 [7-8], 371-72 (1976).

10. F.F. Lange, "Sinterability of Agglomerated Powders," J. Am. Ceram. Soc. 67 [2], 83-9 (1984).

11. F.F. Lange, "Criteria for Crack Extension and Arrest in Residual, Localized Stress Fields Associated with Second Phases," in Fracture Mechanics of Ceramics, Vol. 2, eds., R.C. Bradt, D.P.H. Hasselman and F.F. Lange, Plenum Press (1974), pp. 599-609.

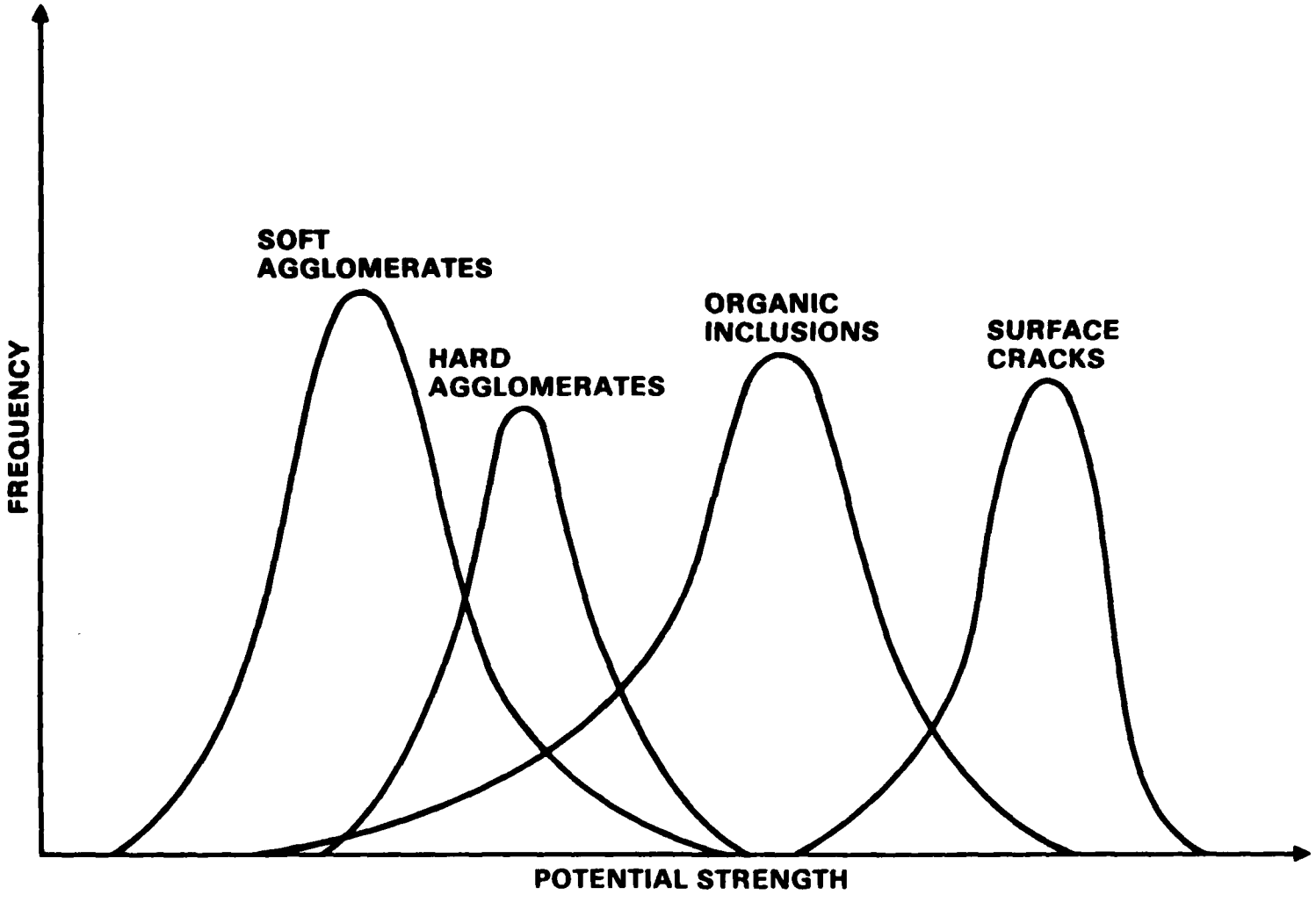

Fig. 1 Schematic of flaw populations controlling the potential strength of certain pressureless sintered transformation toughened ceramics.

TWO-PHASE MIXTURES

SC83-22151

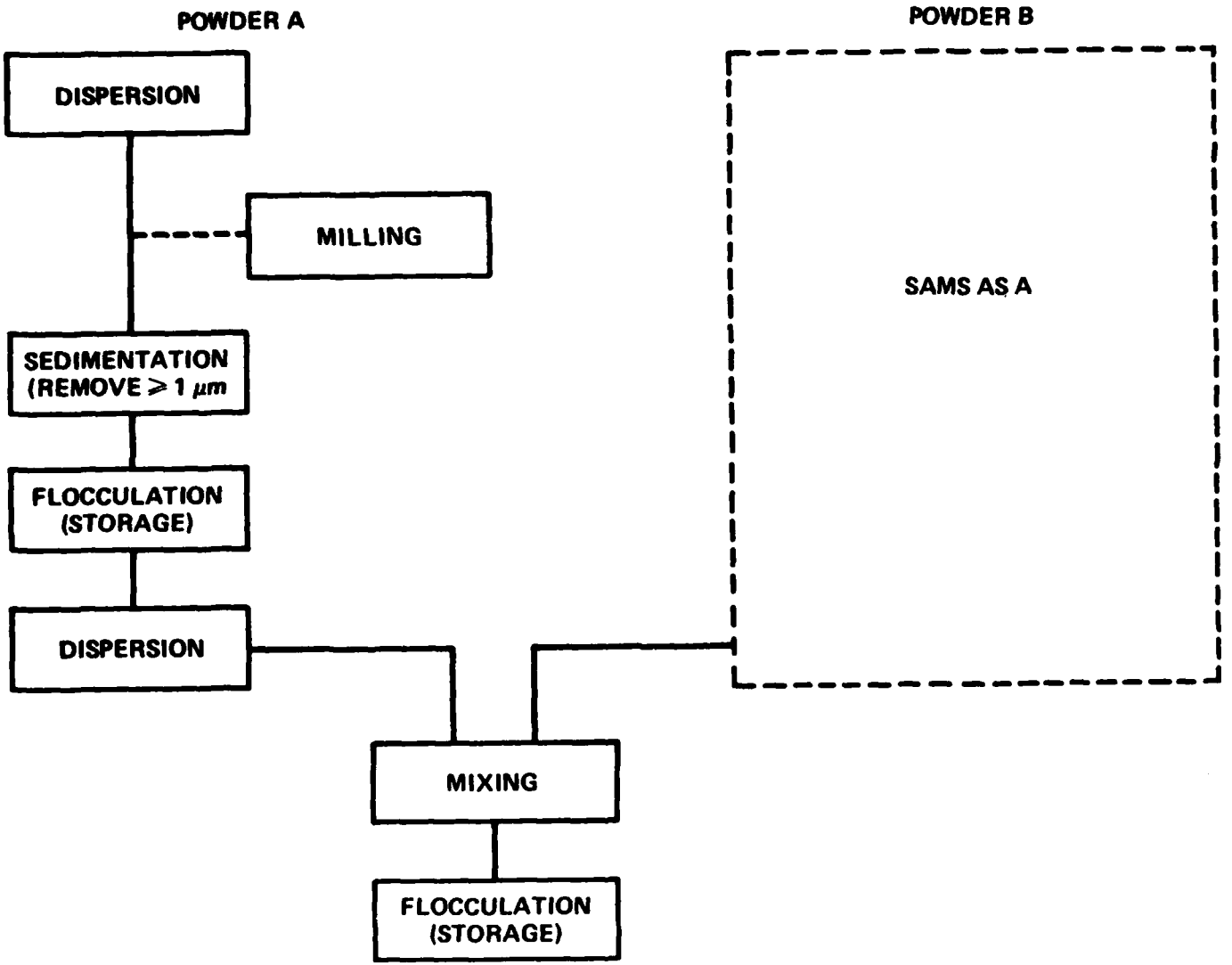

Fig. 2 Flow chart for processing multiphase powder composites which minimize agglomerate size.

SC84-27021

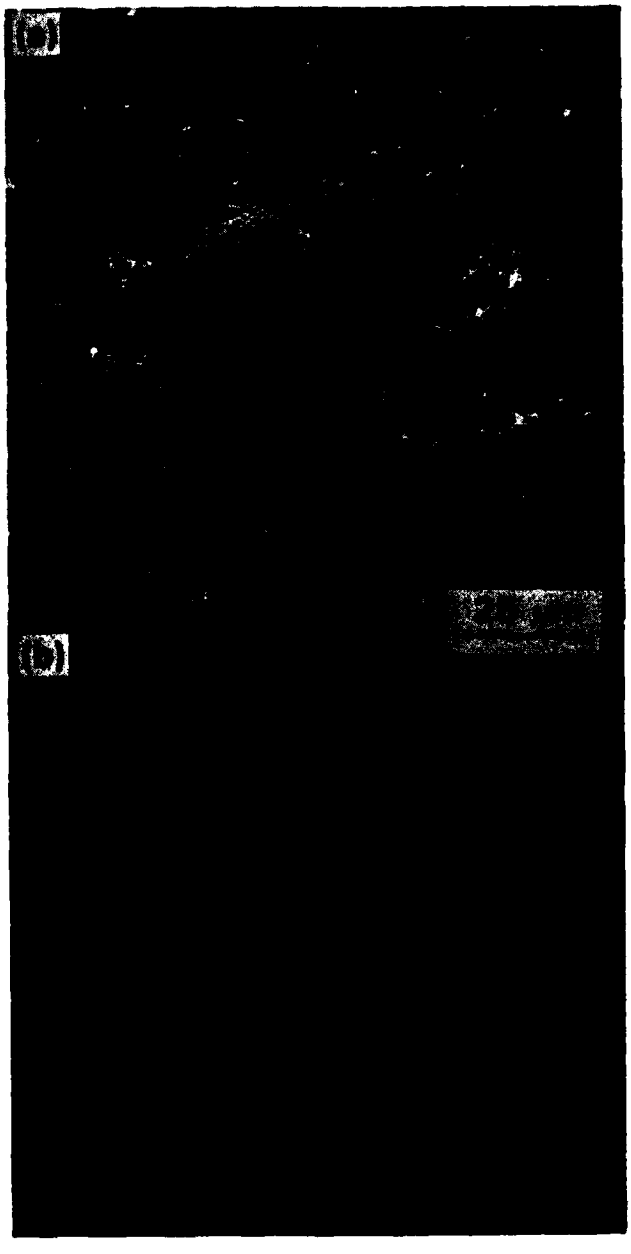

Fig. 3 Large, soft ZrO_2 globular agglomerate at fracture origin: a) secondary electrons, b) backscattered electrons.

SC84-26065

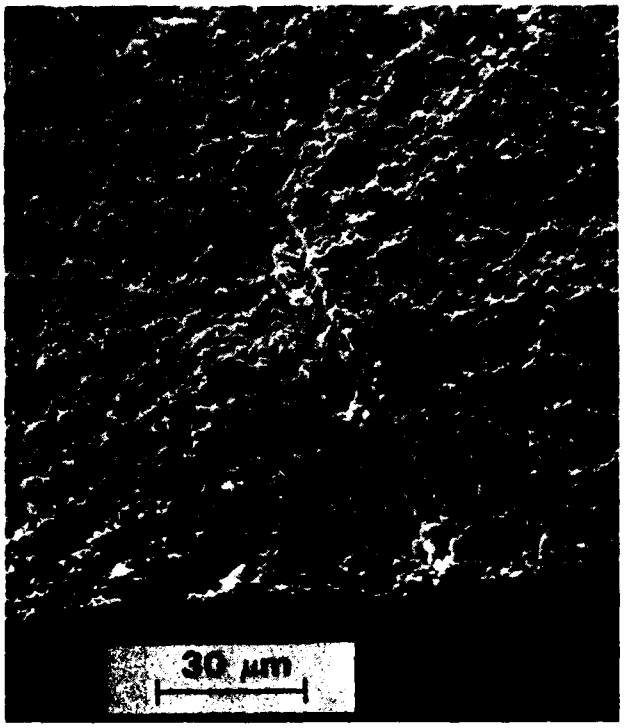

Fig. 4 Void produced by an organic inclusion at fracture origin in a Al_2O_3/ZrO_2 composite.

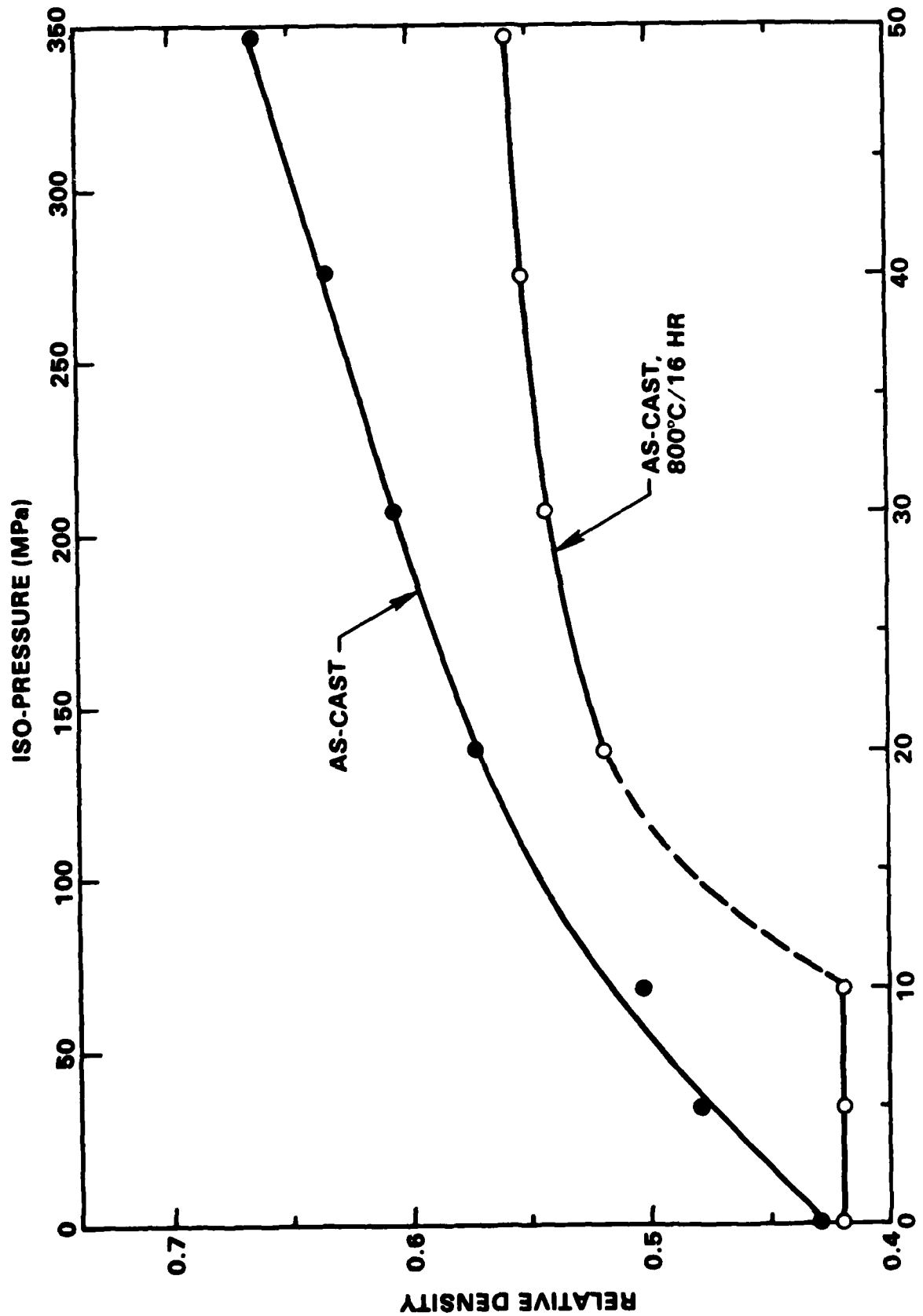

Fig. 5 Increase in bulk density as a function of iso-pressure for both as-cast and presintered (800°C) powder compacts.

SC84-26067

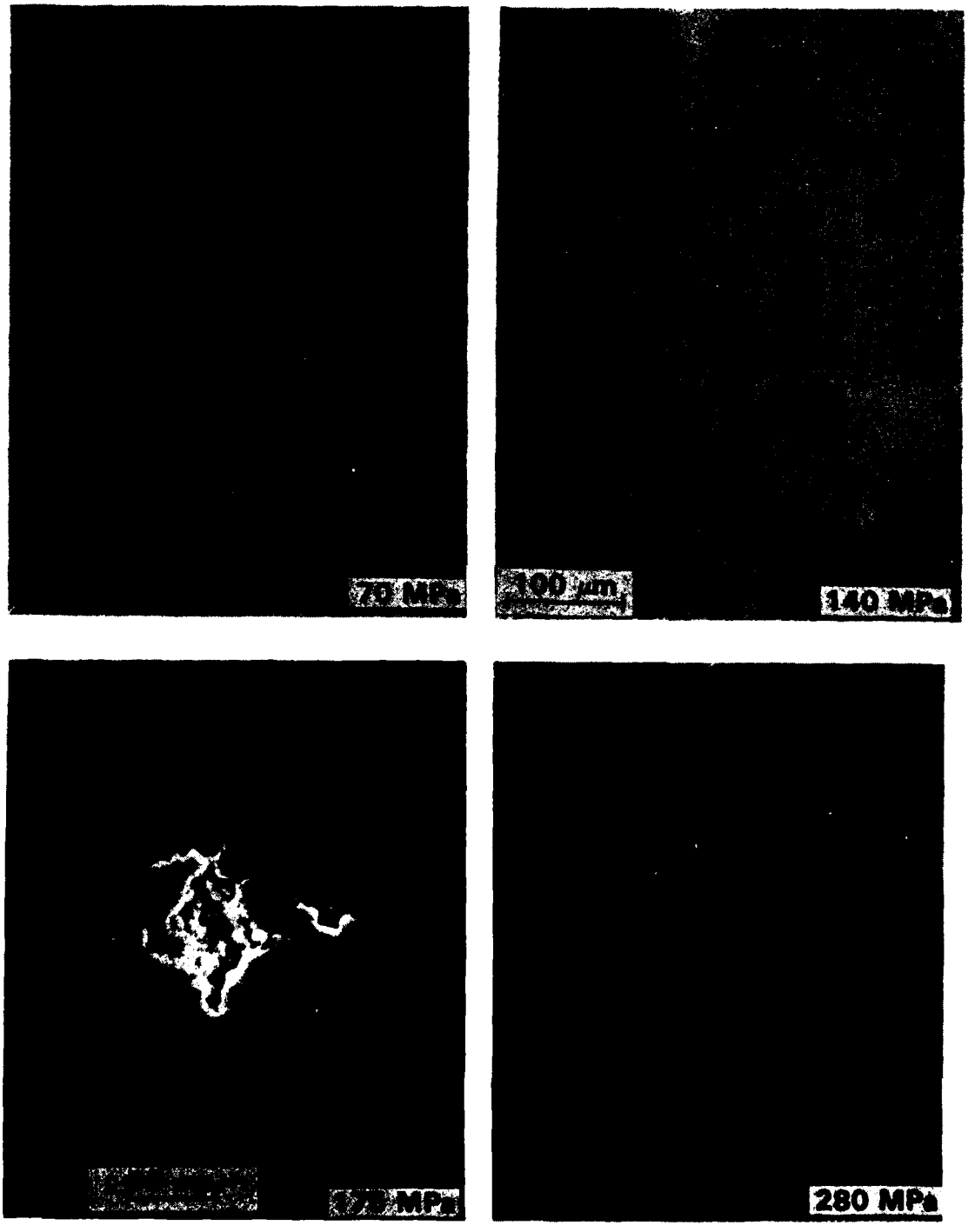

Fig. 6 Morphology changes of voids produced by 50 μm spheres at different iso-pressures on sintered (1600°C/1 h), polished surfaces.

SC84-27022

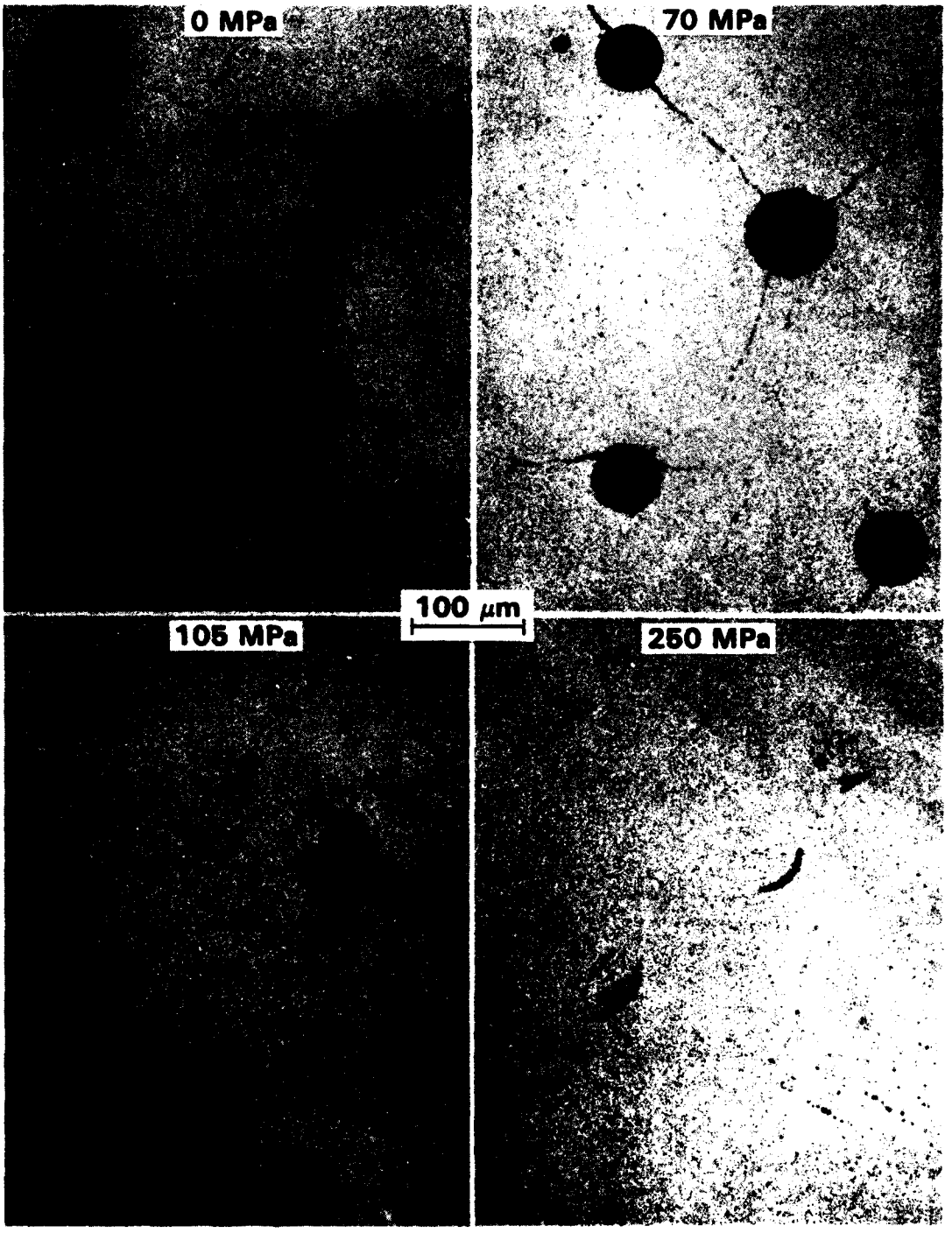

Fig. 7 Effect of iso-pressure on voids produced by 100 μm spheres.

APPENDIX V

PHASE DISTRIBUTION STUDIES USING ENERGY DISPERSIVE X-RAY SPECTRA ANALYSIS

F.F. Lange and M.M. Hirlinger*
Structural Ceramics Group
Rockwell International Science Center
Thousand Oaks, CA 91360

ABSTRACT

A preliminary study was undertaken to determine if EDAX spectra, obtained at different magnifications, might be used to define the phase distribution in a multiphase material. Al_2O_3/ZrO_2 composites were used for the study. EDAX spectra were acquired for a number of arbitrarily selected areas at each magnification using a commercial scanning electron microscope/x-ray detector/multichannel analyzer system. A statistical analysis of the spectra showed that the deviation from the mean phase distribution increased with magnification. These results showed that the smallest area that contained the same phase distribution as the whole specimen could be defined if one first defines an acceptable deviation from the mean. Spectra acquired for the same area suggest that an acceptable deviation is 5% of the mean. Within the limits of multielement detectability, these preliminary results strongly suggest that this EDAX method could be used as a quality assurance tool throughout the processing and fabrication of a multiphase material.

---

* Margret Hirlinger is an undergraduate student in the Physics Department at MIT.

1.0 INTRODUCTION

The distribution of second phases incorporated to aid densification, control microstructure and/or to achieve desired properties is a critical issue in ceramics. Quantitative sterology is certainly a well developed science, but unless the observer is subjective, the techniques are labor-intensive, since electron microscopy is required to observe the microstructures of advanced ceramics. It is reasonable to suspect that information produced by a scanning electron beam other than phase contrast could be used to automate phase distribution determinations. In many cases, the chemistry of different phases within a multiphase ceramic is sufficiently different to enable phase identification by energy dispersion x-ray analysis (EDAX), a common tool used in conjunction with a scanning electron microscope (SEM). In practice, phase identification with EDAX is carried out by increasing the magnification until the area scanned by electrons is within the phase area to be identified. If one were to reduce the magnification from this point (i.e., increase the area scanned), other phases will begin to contribute to the EDAX spectrum. In principal, if one were to continue to reduce the magnification, a spectrum will be obtained from an area that represents the phase distribution of the total sectioned specimen area. This concept suggests that by obtaining EDAX spectra at different magnifications, one might be able to define the smallest area (or volume element) which contains the phase distribution that represents the whole specimen.

An investigation was initiated to study this concept. Two phase Al_2O_3/ZrO_2 composites were chosen for this investigation, since the strongest spectral peaks for the elements aluminum and zirconia are conveniently close in energy (Al $K\alpha_1$ = 1.49 eV and Zr $L\beta_1$ = 2.04 eV), but not overlapping. Four different compositions were analyzed: three (containing 1, 10 and 40 v/o ZrO_2) were processed by a colloid consolidation technique expected to produce a uniform dispersion, and the fourth (containing 30 v/o ZrO_2) was processed to ensure a poor phase distribution. Statistical information was obtained at different magnifications to determine the validity of the method and to establish a technique to use the concept.

2.0 EXPERIMENTAL PROCEDURE

2.1 Material Specimen Preparation

The Al_2O_3* and ZrO_2** powders used to fabricate three of the materials (composites containing 1, 10 and 40 v/o ZrO_2) were prepared, mixed and consolidated by a colloidal method to help insure a uniform phase distribution.[1] To produce a nonuniform phase mixture, powders for the fourth material (Al_2O_3/30 v/o ZrO_2) were simply mixed with a mortar and pestle and consolidated into a cylindrical shape. All materials were sintered at 1600°C for 2 h.

The colloidal method involves separately dispersing each as-received powder in a fluid, sedimenting to eliminate agglomerates > 1 m, mixing the two particulate dispersions together, floccing the two phase dispersion to prevent segregation, consolidating to form a specimen shape, drying to eliminate the fluid phase from the specimen, and then sintering. This method has been detailed elsewhere[2] for fabrication of Al_2O_3/ZrO_2 composites used for grain growth studies.

The dense, sintered materials were sectioned, polished and then thermally etched at 1550°C for 1 h to reveal grain and phase boundaries. Figure 1 illustrates the microstructures and the general phase distribution of the four materials. The polished specimens were carbon coated for the EDAX study.

---

* ALCOA A16SG
** Zincar Inc.

2.2 EDAX Study

The SEM,* x-ray detector,** EDAX spectrometer, multichannel analysis system*** used for this study were nonaltered, commercial instruments used in their usual mode of operation. The carbon coated specimen and detector were positioned to optimize SEM viewing and the acquiring of x-ray spectra for analysis. The filament voltage was 20 KVA. The sensitivity of the multichannel analyzer was selected as 10 eV per channel. Focusing was carried out at high magnification (usually 10,000X) before a magnification and a random area was selected for EDAX data acquisition. Spectra were acquired for a period of 100 s. Using available software, each spectrum was analyzed by first defining the background curve fitting with channel positions in the range between 1.0 to 3.2 keV, which did not record the spectral peaks of either Al or Zr, and then stripping this background from the acquired spectrum. After stripping the background, the number of x-ray photons (counts) were integrated between 1.34 keV and 1.64 keV, and 1.89 keV and 2.19 keV to determine the integrated peak intensity fo the $AlK\alpha_1$ and $ZrL\beta_1$ peaks, respectively.

The fractional ratio of these two integrated peak intensities (Z/(A+Z)) were used in subsequent analyses for characterizing the phase homogeneity. A number of spectra that were obtained at the same magnification areas were selected by randomly moving the specimen. An attempt was made to sufficiently move the specimen so that the new area to be examined did not overlap a previous area. Since single specimens of each material were used in this preliminary analysis of the technique, the number of nonoverlapping areas that could be examined at lower magnifications was reduced due to the specimen size (approximately 5 mm x 5 mm). After acquiring numerous spectra at different magnifications, the data were analyzed to determine the usefulness of the proposed analytical tool.

---

* ETEC Auto Scan
** Princeton Gamma Tech
*** Kevex

The relation between the area scanned (A) and magnification (M) was determined to be $A = (\frac{9.2}{M}\ \mu m)^2$.

Results

Table 1 reports the statistical data obtained from the four materials. Figure 2 illustrates the standard deviation* of Z/(Z+A) normalized by its mean value plotted against magnification. Both Table 1 and Fig. 2 illustrate that SD increases with magnification. Figure 2 also illustrates that the deviation from the mean distribution increases more rapidly with decreasing ZrO_2 content. As reported in Table 1, the deviation from the mean phase distribution can be < 2% when the phase distribution is determined by a series of different area scans at low magnification. Repeated scans of the same area (data not given in Table 1) indicated that the deviation from the mean was < 4%.

Data represented in Fig. 2 show that the deviation from the mean gradually increases with increasing magnification. Definition of the smallest area that represents the mean phase distribution is therefore subjective. That is, one can only choose an area that represents the mean phase distribution by first choosing a deviation from the mean. For example, one might choose a deviation of 5% of the mean. The smallest area which represents the mean distribution within a deviation of ± 5% can then be defined with the data shown in Fig. 2. Using this choice, the smallest area can be defined for the 10 v/o and 40 v/o ZrO_2 materials as $(30\ \mu m)^2$ and $(18\ \mu m)^2$, respectively.

---

* The calculation of the standard deviation assumes a Gaussian distribution of Z/(Z+A). Analysis show that the Z/(Z+A) distribution can strongly deviate from a Gaussian distribution at high magnifications. This deviation is reflected by large deviations of the mean value of Z/(Z+A) relative to the mean value obtained at lower magnifications as shown in Table 1.

Table 1

Statistical EDAX Data

Material (v/o ZrO_2)	Magnification	Number of Spectra	Mean Al (Counts)	Mean Zr (Counts)	Mean Fraction	Standard Deviation	SD/Mean
1	1,000	8	1.66E5	1.40E3	0.0084	0.0013	0.152
	5,000	18	2.05E5	1.62E3	0.0078	0.0022	0.282
	10,000	13	2.02E5	1.25E3	0.0061	0.0036	0.581
	20,000	17	1.93E5	1.43E3	0.0074	0.0063	0.858
	50,000	16	2.01E5	1.90E3	0.0095	0.013	1.389
	100,000	40	2.02E5	1.53E3	0.0076	0.017	2.20
10	100	11	1.51E5	1.87E4	0.1105	0.0018	0.016
	1,000	11	1.53E5	1.86E4	0.1089	0.0025	0.023
	2,000	15	1.36E5	1.72E4	0.1097	0.0046	0.042
	5,000	21	1.59E5	2.13E4	0.1184	0.0075	0.063
	10,000	24	1.74E5	2.12E4	0.1088	0.0128	0.118
	20,000	45	1.64E5	1.98E4	0.1078	0.0240	0.233
	50,000	39	1.71E5	2.31E4	0.1194	0.0457	0.383
	100,000	18	2.40E5	2.67E4	0.0930	0.0800	0.859
	200,000	28	1.35E5	1.30E4	0.0877	0.0952	1.085
40	2,000	18	1.06E5	6.62E4	0.3851	0.0085	0.022
	5,000	16	1.09E5	6.58E4	0.3761	0.0196	0.052
	7,000	18	1.18E5	7.09E4	0.3761	0.0265	0.071
	10,000	15	1.15E5	6.75E4	0.3701	0.0291	0.079
	15,000	17	1.14E5	7.07E4	0.3814	0.0562	0.147
	20,000	12	1.17E5	6.93E4	0.3718	0.0606	0.163
	50,000	29	1.05E5	6.26E4	0.3732	0.0943	0.253
	100,000	15	1.13E5	6.47E4	0.3630	0.1294	0.357
30	100	13	1.55E5	7.52E4	0.3229	0.0312	0.097
	200	12	1.07E5	5.71E4	0.3466	0.0686	0.198
	500	16	1.30E5	5.79E4	0.3077	0.1020	0.331
	1,000	16	1.38E5	6.03E4	0.3011	0.1825	0.606
	2,000	21	1.19E5	6.10E4	0.3614	0.1956	0.541
	5,000	17	1.04E5	7.60E4	0.4174	0.2540	0.609
	10,000	17	1.19E5	6.10E4	0.3300	0.2627	0.796

Discussion

An investigation was undertaken to determine if EDAX could be used to define the phase distribution of a polyphase material. The results suggest that if one first chooses a deviation from the mean value, the smallest area can be defined which represents the mean phase distribution for the chosen deviation. In this manner, materials of the same nominal phase content can be compared to one another to determine their relative phase distributions.

The technique used for this investigation was manual and, therefore, very labor-intensive. In addition, data were collected over a large range of magnification, which was necessary to show the increase in deviation for the current investigation, but is not necessary to define the smallest area which represents the phase distribution within the chosen deviation. With the possible exception of specimen mounting and initial focusing, all of the manual operations used here can be automated, i.e., area selection and magnification change. Once a deviation from the mean is chosen, the range of magnifications needed and the number of area scans could be significantly reduced to obtain the desired information. With these changes, it is reasonable to suggest that the EDAX technique outlined here could be used to define the phase distribution of a material which could be used as a quality inspection tool during the manufacture of a polyphase material in either its consolidated powder state or dense, fired state.

Acknowledgement

Special thanks to D.J. Green and T. Shaw in assisting this work. This work was performed for the Air Force Office of Scientific Research under Contract No. F49620-81-C-0036.

Reference

1. F.F. Lange and M.M. Hirlinger, "Hindrance of Grain Growth in Al_2O_3 by ZrO_2 Inclusions," J. Am. Ceram. Soc. 67, 167 (1984).

SC84-26662

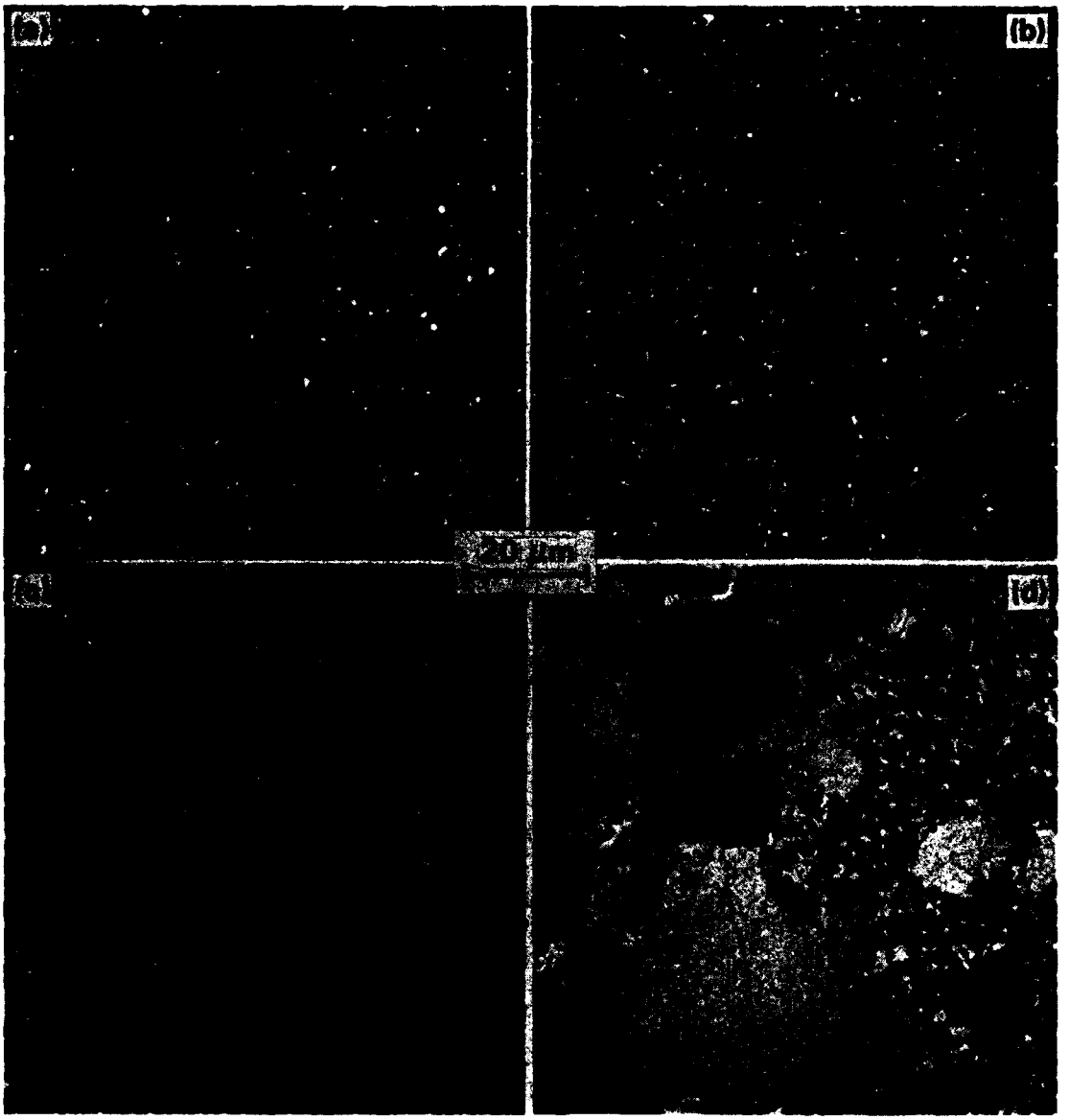

Fig. 1 Backscatter SEM micrographs of the four materials used in the study.

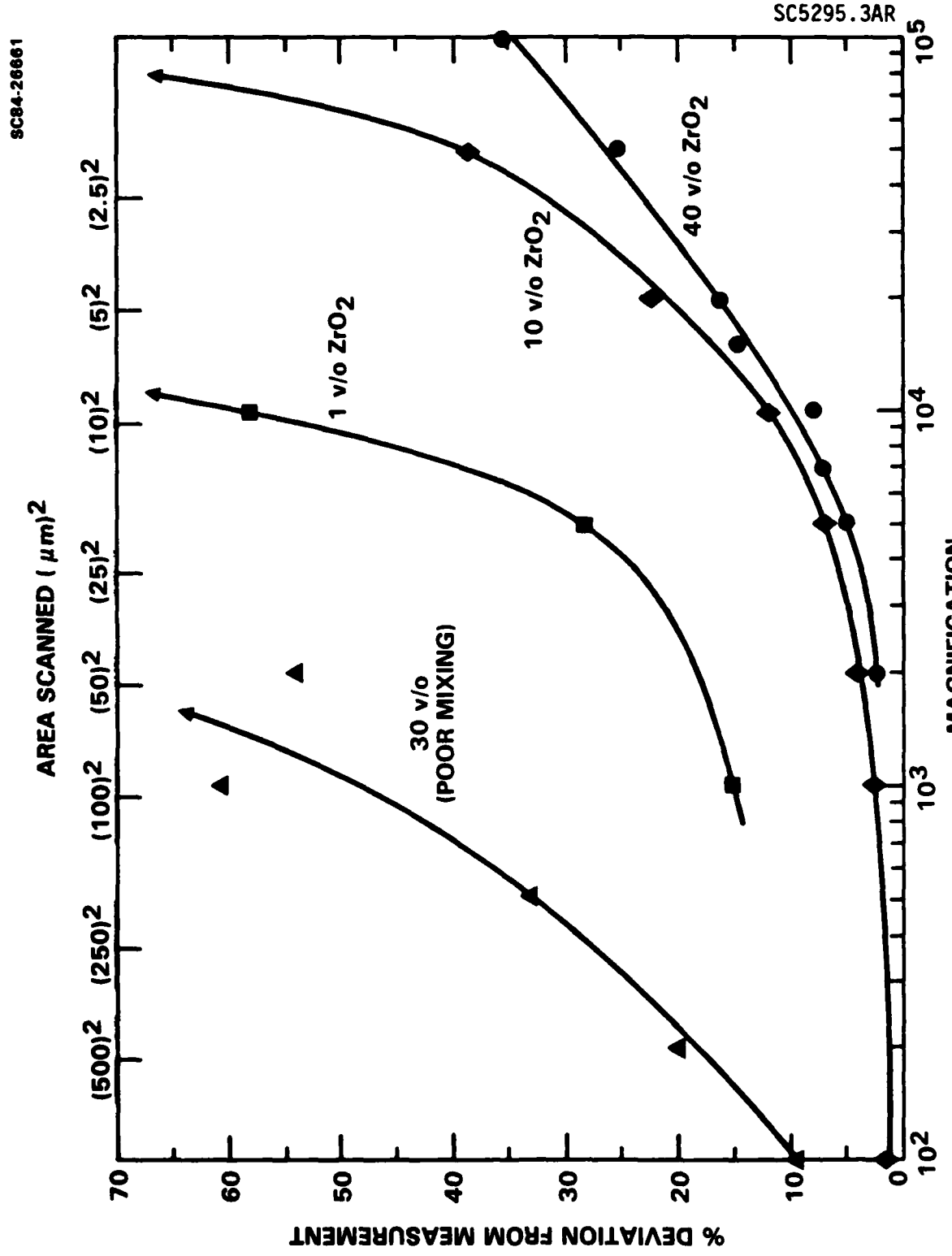

Fig. 2 Percent standard deviation from themean phase distributions vs magnification (or area scanned) for the four material used in the study.

APPENDIX VI

EFFECTS OF ATTRITION MILLING AND POST-SINTERING HEAT TREATMENT ON FABRICATION, MICROSTRUCTURE AND PROPERTIES OF TRANSFORMATION TOUGHENED ZrO

F.F. Lange

Rockwell International Science Center
Ceramics Group
Thousand Oaks, CA 91360

and

H. Shubert, N. Claussen and M. Ruhle

Max Planck Institut fur Metallforschung
Institut fur Werkstoffwissenschoflen

ABSTRACT

The effect of attrition milling and post-sintering heat treatment on the fabrication, phase relations, microstructure and properties of ZrO_2 (+ 2.2 v/o Y_2O_3) powder used to produce a transformation toughened material was examined. Powder used to fabricate the unmilled material was treated and consolidated by a colloidal method. The same powder, treated and consolidated by the same method, but ball-milled in a commercial alumina mill before consolidation, was used to fabricate the milled material. Both materials were sintered at 1400°C/1 h and then heat treated at higher temperatures. Milling introduced Al_2O_3 inclusions (< 1 vol%) and a glass phase (7 to 10 vol%). The milled powder was more difficult to sinter and exhibited more bloating during heat treatment. TEM observations indicated that the larger glass content of the milled material beneficially reduced residual stresses that arose due to thermal contraction anisotropy. A limited Al solid-solubility in the ZrO_2 structure was suspected to cause the milled material to enter the two phase (tetragonal and cubic) field at a lower heat treatment temperature than observed for the unmilled material.

Upon entering the two-phase region, large (presumably cubic) grain heterogeneously nucleated to produce a bimodal grain size distribution which was more pronounced on the surface of the heat treated, milled materials. Large pores produced during heat treatment in the two-phase field were coordinated by larger grains. It is hypothesized that the pores were produced by the release of high pressure oxygen during phase decomposition.

Both fracture toughness (K_c) and hardness of dense, as-sintered materials were unaffected by milling (contamination with Al_2O_3 and glass). Hardness decreased with bloating and the decrease was more pronounced for the milled material. The tetragonal to monoclinic transformation was spontaneous in both materials after heat treating in air at 250°C/16 h. This unwanted transformation phenomena was not observed in vacuum, suggesting it is caused by a reactant present in air, e.g., water vapor.

1. Introduction

Attrition milling, e.g., ball milling, vibro milling, etc., is a customary step practiced in both the research laboratory and the factory to prepare ceramic powders for subsequent steps in fabricating dense shapes by sintering. This practice, originally devised by manufacturers of traditional ceramics (e.g., white wares, refractories, etc.), was the last stage of particle size reduction and was also used to mix the mined, raw materials in preparation for forming the desired powder shapes that could be sintered at a reasonable temperature. For traditional ceramics, impurities introduced during attrition milling were usually insignificant relative to impurities already present in the raw materials. Today, advanced ceramics are being developed for applications ranging from electronic packaging to advance heat engines. Powders used for these new ceramics are commonly produced from purified reactants (e.g., gases, liquids, hydroxides, alkoxides, etc.). Although the crystallite size of these purer powders can be < 1 μm, attrition milling is still used to break apart hard agglomerates formed by partial sintering of the crystallites at the reaction temperature, and also for mixing of second phases. The reduction of agglomerate size is necessary not only to increase sinterability, but also to eliminate (or reduce) the crack-like voids produced by the differential shrinkage of agglomerates relative to the surrounding powder. For these new powders, impurities introduced during attrition milling can be significant relative to the unmilled powder.

Alternate powder treatments, based on the sedimentation of dilute powder/liquid, colloidal suspensions, can be used to eliminate agglomerates greater than a chosen size.[1] Experience suggests that this method results in a greater probability that agglomerates will be eliminated relative to milling. One might also suspect that this colloidal treatment would also result in fewer impurities. To test this hypothesis and to determine the influence of impurities introduced by milling on fabrication and properties, a study was initiated to compare materials fabricated by the colloidal/sedimentation method to the conversional method of attrition milling.

A zirconia powder containing 2.3 mole% Y_2O_3 was chosen for this study, since it can produce a strong, transformation toughened material. A commercial Al_2O_3 based ball mill and milling media* were used because of its common use throughout the ceramic industry and in research laboratories. The Al_2O_3 used to fabricate these mills contains a silicous glass.** Studies of materials produced by the two powder treatment methods included effects of contaminants on phase relations, the low temperature degradation effect in ZrO_2-Y_2O_3 transformation toughened materials, microstructural changes, fracture toughness and high resolution microscopy.

Experimental

The as-received ZrO_2 powder used for this study contained large, hard agglomerates produced during the conversion of $ZrOCl_2$ plus a soluble salt to a $Zr_{(1-x)}Y_xO_{2-\frac{x}{2}}$ ($x = 0.045$ or 2.3 mole%/Y_2O_3) powder at elevated temperatures. The powder also contained large, soft agglomerates. A colloidal treatment was used to break apart the soft agglomerates and to eliminate large, hard agglomerates. This treatment was used to prepare powder for both the unmilled and milled materials.

The colloidal treatment[1] involved dispersing the as-received powder in sufficient water to obtain 3 vol% solids at pH = 2 with HCl, sedimenting the dispersion three times to eliminate all particles and hard agglomerates > 1 m, and then spontaneously flocculating the suspension containing particles and hard agglomerates < 1 m by changing the pH to 7 with additions of NH_3OH. Flocculating concentrates the solids and prevents further mass segregation due to sedimentation during storage. Excessive salts due to HCl and NH_3OH additions were minimized by repeated washing of the flocced material. Washing was per-

---

* Norton Co., Akron, OH, 85% Al O , 11% SiO , 1.2% CaO, 2.0% MgO.
** Purer Al O mills and media are large grain materials and wear at an unacceptable rate.

formed after floccing by removing the clear supernate, adding distilled water, mixing and refloccing without acid or base additions. Table I lists the Y_2O_3 content and impurities observed in this powder after the above treatment.

A portion of the flocced slurry was redispersed by adding HCl to lower the pH to 2. This portion was ball milled in a Al_2O_3 mill for 16 h, poured into a plastic container, and immediately reflocced by changing the pH to 7 with NH_3OH.

Cylindrical specimens of both the unmilled and milled flocced slurries were consolidated by filtration (slip casting on plaster). After drying, the specimens were iso-pressed at 350 MPa and then sintered at 1400°C for 1 h. After sintering, all specimens were diamond ground and polished. Different specimens of each material (viz, unmilled and milled) were heat treated for 1 h at temperatures ranging from 1350°C to 1650°C. Densities were determined by the Archimedes method, phases were determined by x-ray diffraction

Table I

Cation Content* of Unmilled ZrO_2 Powder

Ca	4000
Hf	2.1%
P	1180
Si	760
Ti	1000
Y_2O_3	4.10% (2.28 mole %)

* Analyses in ppm unless otherwise noted.
Cations < 500 ppm not shown.
Courtesy of Teledyne, Wah Chang Albany

analysis (XRD), the polished and heat treated surfaces were observed with the scanning electron microscope (SEM), the hardness (H) and critical stress intensity factor (Kc) were determined as a function of heat treatment using an indentation technique[2] (20 Kgm load), and both as-sintered materials were ion

thinned for high resolution transmission electron microscopy (TEM) observations. After observations were made on the heat treated surfaces, the interior was examined with the SEM after diamond grinding, polishing and thermal etching at 1350°C/1 h. Different heat treated specimens were heated to 250°C for periods of 16 h in air and rough vacuum (10^{-2} Torr), and examined by XRD for phase content.

3. Results

3.1 Density

Previous studies have shown that the ZrO_2 (+ 2.2 m/o Y_2O_3) powder treated and consolidated in the manner outlined above could be sintered at 1400°C/1 h to achieve a density > 98% of theoretical (ρ_t = 6.07 gm/cm^3) without the iso-pressing step.[1] Preliminary work for this study showed that porous materials with densities < 5.50 gm/cm^3 were obtained when the powders were milled, as described above, before consolidation. Iso-pressing, prior to sintering, was used to help remedy this situation. Iso-pressing increases the bulk density of the dried powder compact from 33% to 48% of the theoretical density. This observation suggests that the milled powders were less sinterable than the unmilled powders.

Densities are reported in Table II as a function of heat treatment temperature. A density of > 98% of theoretical (ρt = 6.07 g/cm^{-3}) could be obtained for the unmilled powder sintered at 1400°C/1 h, whereas the milled powder resulted in a significantly lower density. SEM observations of sectioned and polished surfaces of milled material sintered at 1400°C/1 h did not reveal significant porosity. As reported in the subsequent section, the milled material contained a small amount of Al_2O_3 (< 1 v/o) and a significant amount of a glass. Based on the observations of the insignificant porosity and the significant glass content, it was concluded that the glass was the principal cause for the lower density. Assuming that the density of the glass

lies between 2.2 gm/cm^3 and 3.5 gm/cm^3, the volume fraction of the glass in the milled material was calculated* to lie between 0.07 and 0.10, respectively.

As reported in Table II, the density of both materials increased slightly when heat treated at 1450°C/1 h. Heat treatments at higher temperatures resulted in a decrease in density, which was more pronounced for the milled materials. Since all heat treated specimens were presintered at 1400°C/1 h, the loss of density at heat treatment temperatures > 1450°C must be caused by a bloating phenomenon, i.e., the release of a high pressure gas. Observations of sectioned and polished specimens showed the development of large, spherical pores which increased in size with heat treatment temperature. For the same heat treatment temperature, the pores were larger for the milled material. Figure 1 illustrates these pores for the milled material heat treated at 1650°C/1 h. Pores were not observed on the polished and heat treated surfaces; sectioning showed that a 20 μm to 30 μm surface layer was pore-free.

3.2 Phase Content

Figure 2 is a schematic of the portion of the unconstrained ZrO_2-Y_2O_3 phase diagram of interest here. Although several investigations have suggested the positions of the various phase boundaries,[3,4] their exact positions are not known in detail. It is well known that the tetragonal (t) structure can be elastically restrained from transforming upon cooling to room temperature if certain conditions, viz, elastic modules of constraining matrix, grain size and alloying (e.g., Y_2O_3) content are satisfied.[5] The tetragonal phase is the toughening agent in these transformation toughened materials.

* Volume fraction of glass = $\dfrac{(\rho_{specimen} - \rho_{ZrO_2})}{(\rho_{glass} - \rho_{ZrO_2})}$.

Only the t phase could be detected in the as-sintered materials. The monoclinic (m) phase was never observed by XRD in the as-sintered or heat treated materials unless their surfaces were diamond ground. It is well known that surface grinding can stress-induce the t → m transformation.[6]

As reported in Table II, the cubic (c) phase was observed in the heat treated materials. For the ZrO_2/Y_2O_3 composition, the cubic phase can be distinguished by XRD by diffraction peaks that lie between tetragonal (hkl) peaks for h, k ∝ l, e.g., the (311) and (113) tetragonal peaks.[4] The cubic phase was first observed at 1450°C for the milled material and at 1500°C for the unmilled material. For both materials, the fraction of cubic phase increased with heat treatment temperature. The occurrence of the cubic phase is consistent with the phase diagram (Fig. 2) which shows that the single phase tetragonal initially fabricated at lower temperatures will decompose into two new compositions with tetratonal (t') and cubic (c) structures, respectively, upon entering the two phase field. Since the decomposition of the initial tetragonal composition requires diffusion of Zr, Y and O, the cubic composition can easily be retained for XRD examination upon cooling to room temperature.

SEM examination of the milled materials also revealed large Al_2O_3 particles, one of the contaminants introduced during milling, as shown in Fig. 3. The Al_2O_3 particles are easily observed with SEM due to much lower atomic number of Al relative to Zr.

High resolution TEM showed that both unmilled and milled materials contained a silicious glass phase, as shown in light and dark field micrographs in Fig. 4. The dark field micrographs were obtained by imaging the electrons scattered by the glass which enhances the contrast between the glass and crystalline phases. Milled material contained large pockets of glass, typical of Fig. 4b, whereas the much smaller pockets in the unmilled material were confined to three and four grain junctions, typical of Fig. 4a. Glass was also present at all the grain boundaries observed in the milled material

Table IIa

Unmilled ZrO_2 (2.3 m/o Y_2O_3) Material

Heat Treat Temp. (°C)	Density (gm/cm^3)	Phases	Grain Size** (μm)	H (GPa)	K_c (MPa $\cdot m^{1/2}$)
1350	5.99	t	0.30	11.7	5.80
(1400)*	5.99	t	--	--	--
1450	6.07	t	0.31	12.1	5.80
1500	5.99	t + c	0.52	12.0	5.85
1550	5.97	t + c	0.58	11.7	5.88
1600	5.93	t + c	0.68	11.6	6.25
1650	5.85	t + c	--	11.2	6.48
				(10.0)***	(6.68)***

Table IIb

Milled ZrO_2 (2.3 m/o Y_2O_3) Material

Heat Treat Temp. (°C)	Density (gm/cm^3)	Phases	Grain Size** (μm)	H (GPa)	K_c*** (MPa $\cdot m^{1/2}$)
1350	5.76	t	0.29	11.8	6.00
(1400)*	5.76	t	--	--	--
1450	5.81	t + c	0.34	11.1	5.86
1500	5.66	t + c	0.44	10.3	6.07
1550	5.54	t + c	0.72	9.5	6.06
1600	5.37	t + c	--	8.7	5.95
1650	5.25	t + c	--	7.8	6.28

* No heat treatment.
** Smaller grains in bimodal distribution only.
*** Section surface measurements.

and most (if not all) boundaries in the unmilled material. Note the rounded grains in the milled material (Fig. 4b) indicative of a large liquid content at the sintering temperature, relative to the straighter boundaries in the unmilled material.

Energy dispersion x-ray analysis (EDAX) showed that Si, Al and Y were present in the glass, indicating that some of the Y diffused from the ZrO_2 into the liquid silicate during fabrication. The ZrO_2 in the milled material was also observed to contain a detectable amount of Al, indicative of some reaction between the ZrO_2 and Al_2O_3 or glass during sintering.

The most interesting TEM observation concerned differences in the strain fields between the two materials. The unmilled material was highly strained, making imaging much more difficult due to strain contrast. Much of the thin foil of the unmilled material had disintegrated due to the t → m transformation during ion milling. Grain boundary cracks were frequently observed between untransformed t grains (see arrow in Fig. 4a). By contrast, the grains in the milled material contained smaller strains and were easier to image. This observation strongly suggests that the larger amount of glass (viscous liquid at higher temperatures) in the milled material relieves much of the residual stresses developed during cooling due to the anisotropic thermal contraction of the tetragonal ZrO_2 grains.

3.3 Grain Growth

The grains in both materials sintered at 1400°C/1 h, sectioned, polished and thermally etched at 1350°C were nearly identical in average size (0.3 μm) and had a relatively narrow size distribution. A bimodal distribution developed at higher heat treatment temperatures. The development of the bimodal distribution (first observed at 1450°C for milled material and 1500°C for unmilled material) was much more pronounced for the milled material. Figure 5a illustrates the subtle development for the unmilled material between 1450°C to 1550°C, and in Fig. 5b, the more pronounced development for the milled material over the same temperature range. At the highest heat treatment

temperature (1650°C/1 h), the large grains (~ 10 μm) completely covered the surface of the milled material. For the same temperature, the bimodal distribution and average size of the largest grains (~ 5 μm) remained the same as that shown in Fig. 5a at 1550°C. Table I reports the average size of the smaller grains within the bimodal distribution as measured by the line intercept method without correction for either grain volume or shape. These values may be overestimates, since pockets of smaller grains had to be selected that occasionally contained large grains.

Although the heat treated surfaces of the two materials were very different, grain size and distribution of sectioned surfaces thermally etched at 1350°C/1 h were undistinguishable, and were identical to that of the unmilled materials shown in Fig. 5a. The pores developed at higher heat treatment temperatures were coordinated by larger grains, as shown in Fig. 6.

Another reason to suspect that the large grains are cubic is the frequent observation at higher temperatures (> 1600°C) that smaller grains have been included during the growth of larger grains. This observation is shown in Fig. 7 for the case of the unmilled material. The smaller grains (assumed to be the tetragonal phase) are also located at three (or four) grain junctions, strongly suggesting that they impede the growth of the larger cubic grains, as observed for the other two phase materials.[7]

3.4 Fracture Toughness and Hardness

Fracture toughness (K_c) measurements were made as a function of heat treatment temperature to determine if K_c would increase with grain size, as suggested by theory,[5] and measurements on other forms of transformation toughened ZrO_2 materials.[8] Hardness values are a by-product of the indentation technique used to measure* K_c.

---

* This technique requires knowledge of the material's elastic modules, which was assumed to be 207 GPa for all materials regardless of density.

Indentation K_c measurements were made on the outer surfaces of the thermally treated unmilled material and on the sectioned surfaces of the milled material. Average values, reported in Table II, indicate that the fracture toughness of the two as-sintered materials are nearly identical (5.8 and 6.0 MPa • $m^{1/2}$). K_c changed little (< 10%) with heat treatment temperature.

Table II also reports that the hardness (H), measured on the dense surface (unmilled material), only decreases by ~ 8% with increasing temperature, despite the increased porosity of the underlying bulk material. The large decrease in hardness (~ 35%) for measurements of the sectioned, milled material more strongly reflects the increasing porosity with heat treatment temperature.

3.5 Spontaneous t → m Transformation at 250°C

Kobayashi et al[9] and other workers in Japan[10,11] have shown that tetragonal ZrO_2-Y_2O_3 compositions can undergo a spontaneous t → m transformation when heat treated in a temperature range of ~ 200°C to ~ 350°C. This phenomenon can be avoided with Y_2O_3 contents > 3.0 v/o if the grain size is < 0.5 μm. Since one possible explanation of this degrading phenomenon could be a stress corrosion effect, i.e., loss of constraint by slow extension of cracks through the glass phase, experiments were initiated to study this phenomenon with the two materials that contain quite different amounts of glass.

Preliminary experiments were carried out by heat treating the two materials at 250°C in air for 16 h. Both materials exhibited significant t → m transformation for this heat treatment condition, as determined by XRD analysis of the surface. To determine if the phenomenon was caused by a reaction with the environment, a second set of specimens were heated at 250°C in a rough vacuum (10^{-2} Torr) for 16 h. For this condition, a trace of monoclinic was detected on the surface of the milled material, whereas it was not for the unmilled material. These same specimens were then subjected to an air environment at 250°C/16 h, resulting in a significant t → m at the surface.

4. Discussion

As expected, milling unavoidably introduced contaminants, viz. large Al_2O_3 inclusions, and a large fraction of glass. For the ZrO_2 (+ 2.3 m/o Y_2O_3) studied, the contaminants altered sinterability, bloating behavior, phase relations, grain growth and residual stresses. Although not studied, the large Al_2O_3 inclusions can also be considered as an unwanted flaw population.

4.1 Sinterability

The decrease in sinterability of the milled material was surprizing, i.e., one would expect the larger volume fraction of silicate liquid to increase the sinterability of ZrO_2. The authors have no consistent explanation of this observation.

4.2 Bloating

The bloating phenomenon, which must be caused by the release of a high pressure gas, was accentuated in the milled material. Here, the higher volume fraction of the viscous silicate will allow a greater deformation rate during gas release, a shorter period for pores to equilibrate their internal pressure with the external environment, and therefore larger pores which result in a greater loss in density. A possible cause for the bloating phenomenon will be discussed below.

4.3 Phase Relations

As reported, the cubic structure was first detected in the milled material at a temperature 50°C lower than for the unmilled material. That is, the milled material crossed into the two phase (t' + c) region at a lower temperature relative to the unmilled material. A limited Al solid-solubility was observed in the milled (Al_2O_3 contaminated) material. If the limited solid-solubility of Al^{+3} has a similar effect as Y^{+3} in the ZrO_2 structures, the milled material would contain a greater equivalent amount of Y_2O_3 (i.e., Y^{+3} +

Al^{+3}). The net effect of both Y^{+3} and Al^{+3} would cause the milled material to cross into the two phase region at a lower temperature relative to the Al-free, unmilled material.

4.4 Grain Growth

Grain growth in both materials was initiated by the occurrence of abnormally large grains. This occurrence coincided with observation of the cubic phase, strongly suggesting that the larger grains are the cubic phase, which will be the hypothesis used to discuss the grain growth phenomena.

One should first remember that the equilibrium partitioning of the original tetragonal (t) phase into the t' and c phases requires the interdiffusion of all atomic species (viz, Zr, Y(Al) and O). That is, the new tetragonal phase (t') is enriched with Zr and O and depleted of Y, whereas the new cubic phase is enriched with Y and depleted of Zr and O. Second, the nucleation and the growth of cubic grains are driven by a chemical energy free change (phase partitioning); usual grain growth is driven by a surface free energy change (i.e., eliminating grain boundaries).

The heterogeneous nucleation and growth of the presumably larger cubic grains suggests that chemical equilibrium was not maintained during phase partitioning, as expected if the cubic phase were to precipitate within the tetragonal grains (or at grain boundaries). Thus, heterogeneous growth of the cubic phase suggests that stoichiometry is not maintained during the growth of the cubic phase. Since the cubic phase must reject oxygen during growth, which may not be totally absorbed by surrounding tetragonal grains due to the slower mobility of the Zr and Y, one could expect oxygen to be liberated during the observed phase partitioning. (It should be noted that pure ZrO_2 spontaneously loses oxygen in low oxygen partial pressure environments,[12] e.g., vacuum.) One might, therefore, expect to observe a predominance of larger cubic grains at free surfaces and the formation of voids. This argument is certainly speculative, but consistent with the observed facts.

4.5 Residual Stresses

Residual stresses that arise during cooling by thermal contraction anisotropy can produce microcracking, either during cooling itself or upon subsequent tensile stressing. The magnitude of these residual stresses not only depend on the coefficient of differential thermal contraction, but also on stress relaxation phenomena. It is quite obvious that the large glass content in the milled material beneficially relaxes residual stresses during cooling. This observation has many implications with regard to engineering with stronger and more wear-resistant ceramics for lower temperature use.

4.6 Fracture Toughness and Hardness

Both K_c and H were nearly identical for the two as-sintered materials, suggesting that the larger glass content in the milled material has little or no effect on these properties.

The size of the tetragonal grains, presumed to be the smaller grains in the bimodal distribution, on K_c is unclear. K_c does increase at the higher heat treatment temperatures, but the complexity of the microstructural changes, viz, grain size and phase composition and the unaccounted changes in elastic modulus used for the K_c calculation preclude any direct correlation at the present.

4.7 Transformation at 250°C

Since both materials contained a glass phase, the effect of the glass on the low temperature (250°C) t → m transformation phenomenon (e.g., as through a stress corrosion mechanism) is still unclear. Certainly, the results show that the much larger glass content in the milled material did not significantly influence this transformation phenomenon. The experiments did show that the air environment is a major factor, and further experiments are needed to isolate the particular reactant (or catalysis) in the air that triggers this unwanted transformation phenomenon.

Acknowledgement

The technical work of B. Davis is certainly appreciated. A portion of this work was performed while F. Lange was working at the Powder Metallurgy Laboratory at the Max Planck Institute für Metallforschung in Stuttgart. Work was performed under AFOSR Contract No. F49620-81-C-0036.

References

1. F.F. Lange and B.I. Davis, "Sinterability of ZrO_2 and Al_2O_3 Powders: The Role of Pore Coordination Number Distribution," Zirconia II Conf. Proc., Stuttgart, June 1983, in press, Am. Ceram. Soc.

2. A.G. Evans and E.A. Charles, "Fracture Toughness Determinations by Indentation," J. Am. Ceram. Soc. 59, 371 (1976).

3. K.K. Srivastava, R.N. Patil, C.B. Choudhary, K.V.G.K. Gokhale and E.C. Swobaro, "Revised Phase Diagram of the System ZrO_2-$YO_{1.5}$

4. A.G. Scott, "Phase Relationships in the Zirconia-Yttria System," J. Mat. Sci. 10, 1527 (1975).

5. F.F. Lange, "Transformation Toughening: Parts 1-5," J. Mat. Sci. 17, 225-263 (1982).

6. D.J. Green, F.F. Lange and M.R. James, "Factors Influencing Residual Surface Stresses Due to a Stress-Induced Phase Transformation," J. Am. Ceram. Soc. 66, 623 (1983).

7. F.F. Lange and M.M. Hirlinger, "Hindrance of Grain Growth in Al_2O_3 by ZrO_2 Inclusions," J. Am. Ceram. Soc. 67, 167 (1984).

8. M.V. Swain, R.H. Hannink and R.C. Garvie, "The Influence of Precipitate Size and Temperature on the Fracture Toughness of Calcia and Magnesia Partially Stabilized ZrO_2," Fracture Mech. of Ceramics, Vol. 6, eds., R.C. Bradt, A.G. Evans, D.P.H. Hasselman and F.F. Lange, Plenum Press (1983), p. 339.

9. K. Kobayashi, H. Kuwajima and T. Masaki, "Phase Change and Mechanical Properties of ZrO_2-Y_2O_3 Solid Electrolyte After Aging," Solid State Ionics 3/4, 489 (1981).

10. M. Watanabe, S. Iio and I. Fukuura, "Aging Behavior of Y-PSZ," ibid, Ref. 1.

11. M. Matsui, T. Soma and I. Oda, "Effect of Microstructure on Strength of PSZ Components," idid, Ref. 1.

12. R. Ruh and H.J. Garrett, "Nonstoichiometry of ZrO_2 and its Relation to Tetragonal-Cubic Inversion in ZrO_2," J. Am. Ceram. Soc. 50, 258 (1967).

SC84-27023

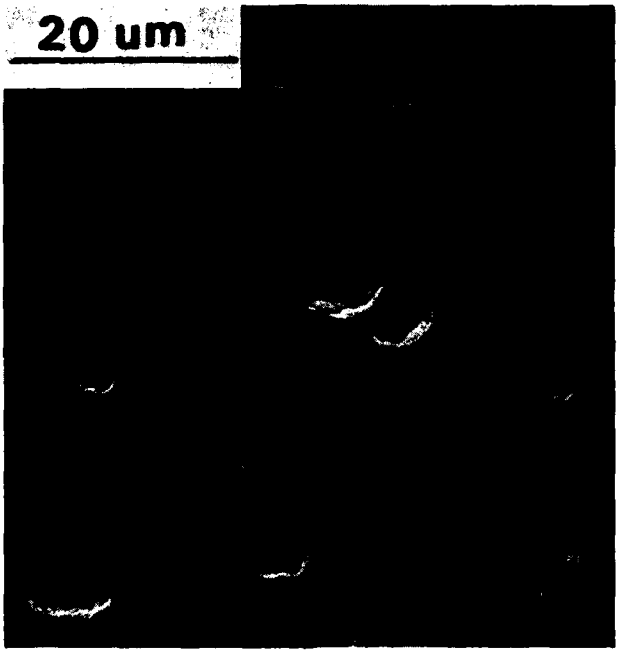

Fig. 1 Bloating voids produced in the milled material heat treated at 1650°C/1 h. Dark areas are Al_2O_3 contaminated grains.

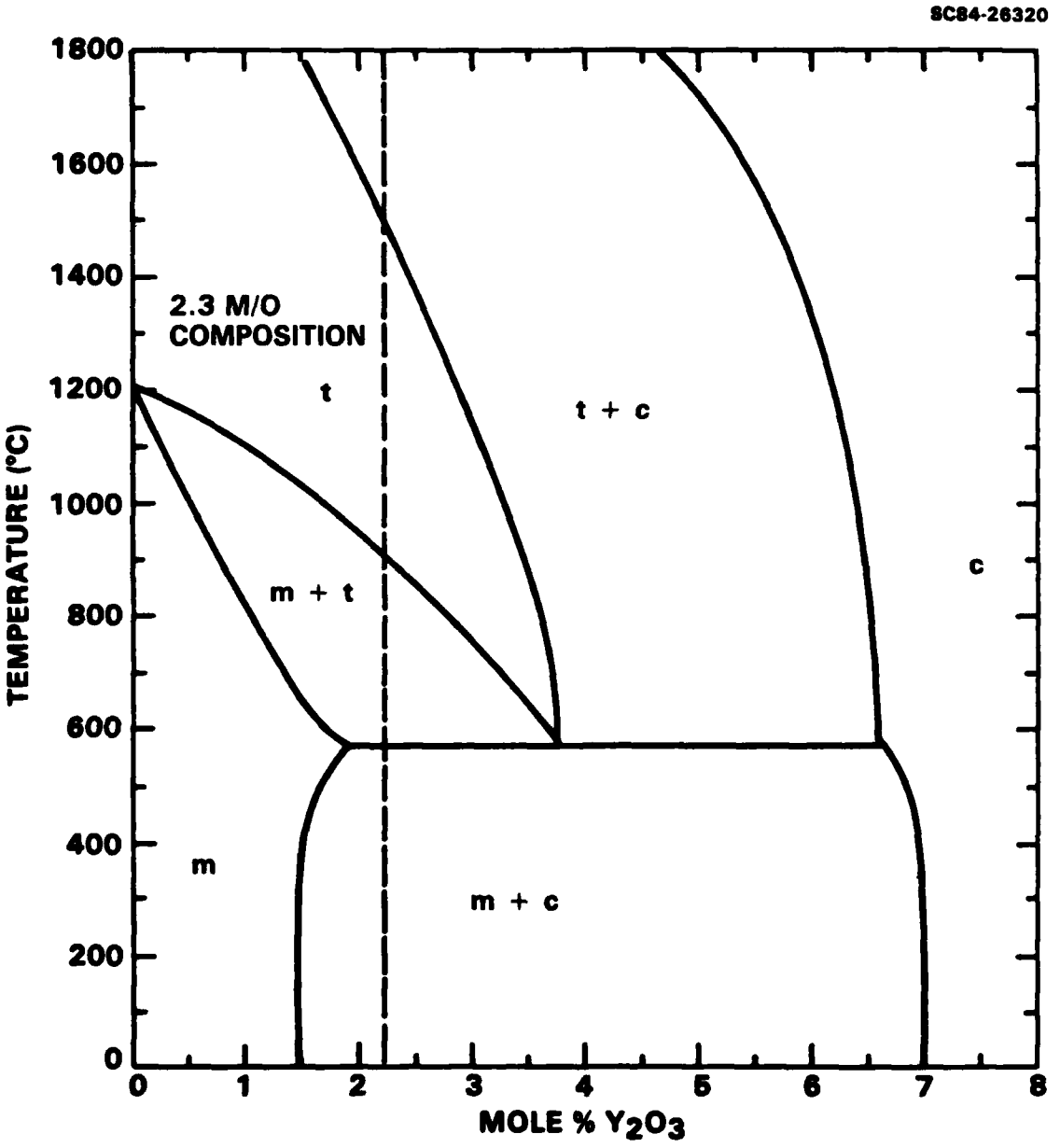

Fig. 2 Portion of ZrO_2-Y_2O_3 binary system.[3,4]

SC84-27024

Fig. 3 Distribution of Al_2O_3 grains introduced during milling.

SC84-27025

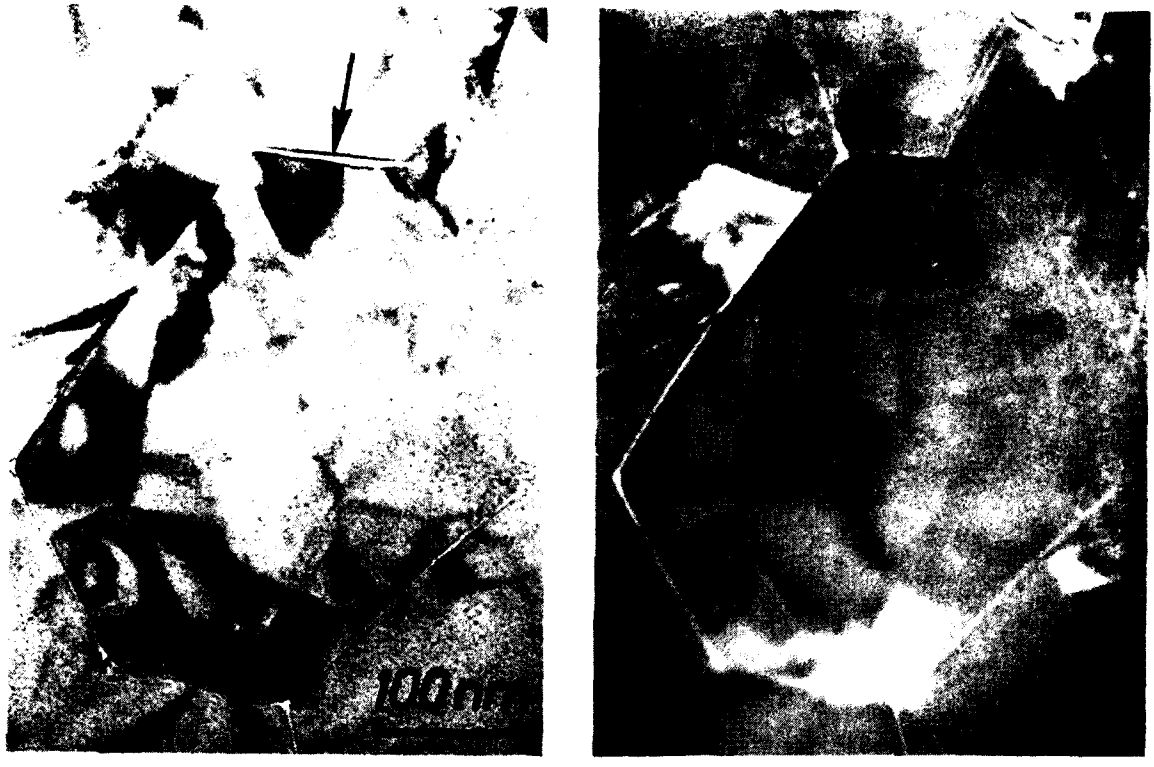

SC84-27026

(a)

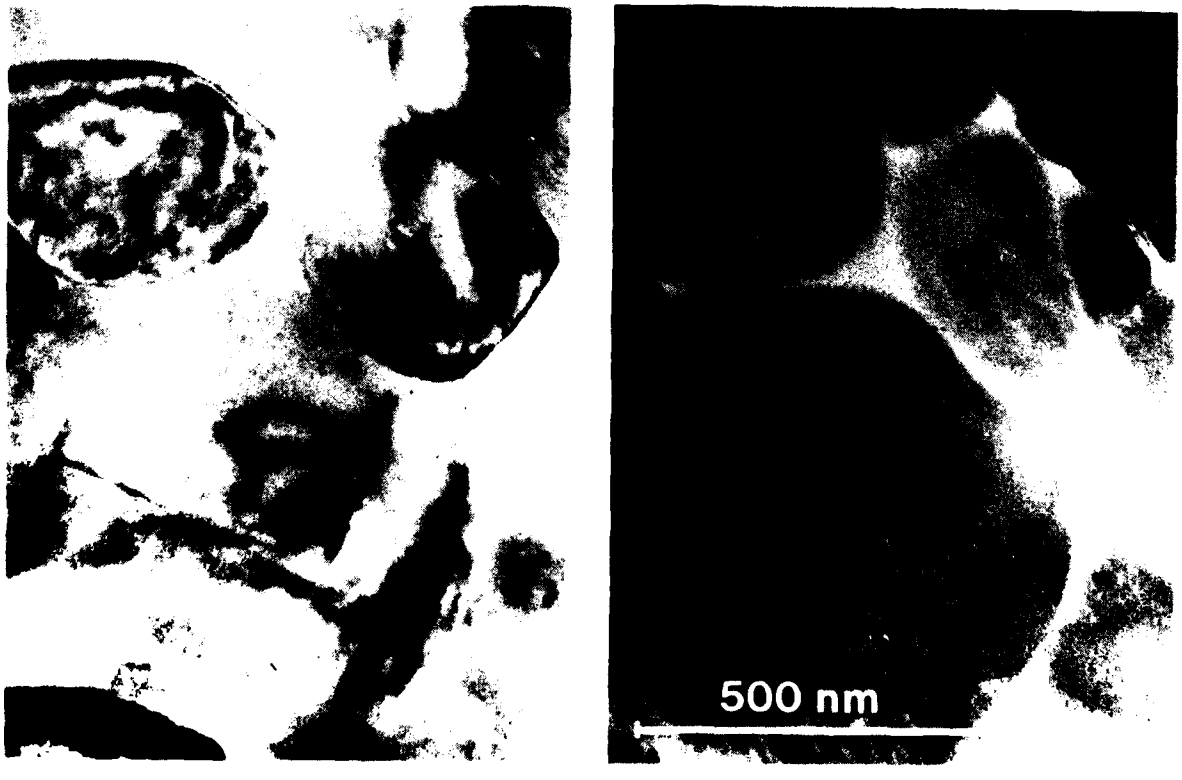

(b)

Fig. 4 a) Unmilled, sintered ZrO_2 (+ 2.3 m/o Y_2O_3) material (arrow points to crack), b) milled, sintered ZrO_2 (+ 2.3 m/o Y_2O_3). Both a) and b) show light and dark field images to indicate glass.

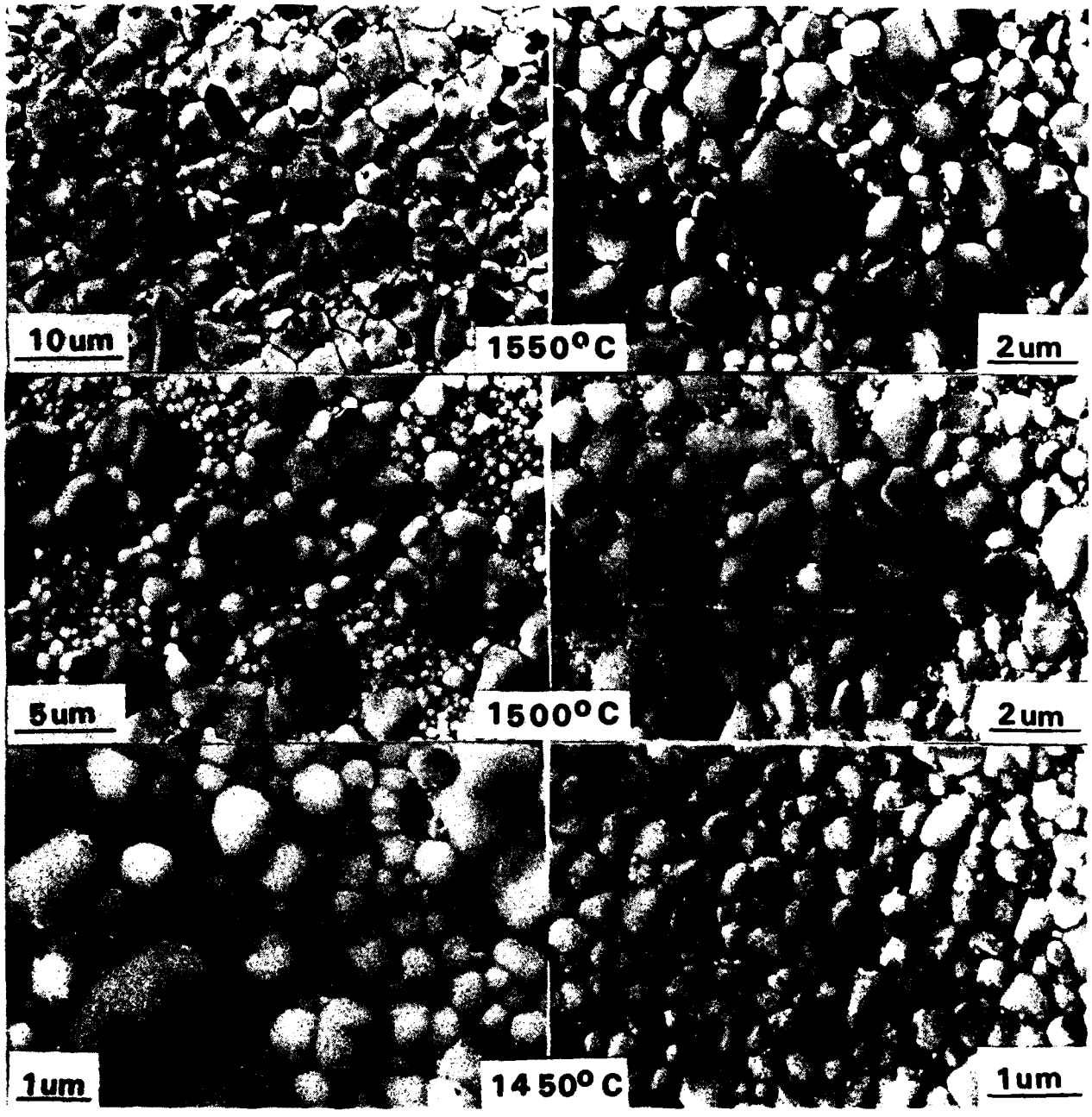

Fig. 5 Grain structures of polished and heat treated materials. Left column: milled material (dark grains are Al_2O_3); right column: unmilled material.

SC84-27028

Fig. 6 Void produced by bloating in milled material showing larger coordination grains.

SC84-27029

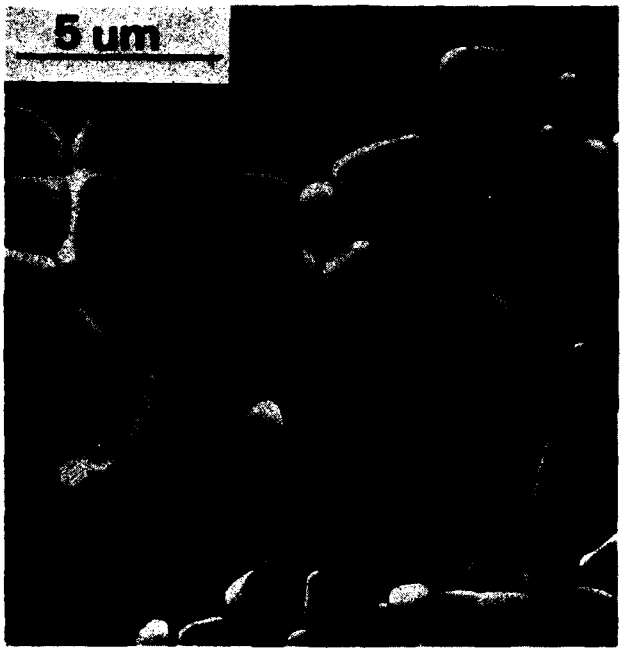

Fig. 7 Grain structure of unmilled material (heat treated at 1650°C/1 h) showing included smaller grain.